LOW REYNOLDS NUMBER AIRFOIL AERODYNAMICS AND PLANE JET

WANG SHU

MPhil

The Hong Kong Polytechnic University

2022

The Hong Kong Polytechnic University

Department of Mechanical Engineering

LOW REYNOLDS NUMBER AIRFOIL AERODYNAMICS AND PLANE JET

WANG SHU

A thesis submitted in partial fulfilment of the requirements for the degree of Master of Philosophy

June 2016

CERTIFICATE OF ORIGINALITY

I hereby declare that this thesis is my own work and that, to the best of my knowledge and belief, it reproduces no material previously published or written, nor material that has been accepted for the award of any other degree or diploma, except where due acknowledgement has been made in the text.

___________________________________ (Signed)

___________WANG Shu______________ (Name of student)

ABSTRACT

This thesis studies the aerodynamics of low Reynolds number flow. A great deal of experimental work is done to investigate the symmetrical airfoil.

The thesis reports the investigation of the aerodynamics of a NACA 0012 airfoil at the chord-based Reynolds numbers (Re_c) from 5.3×10^3 to 2.0×10^4. The lift and drag coefficients, C_L and C_D, of the airfoil, along with the flow structure, were measured as the turbulent intensity T_u of oncoming flow varies from 0.6 % to 6.0 %. The analysis of the present data and those in the literature unveils a total of eight distinct flow structures around the suction side of the airfoil. Four Re_c regimes, i.e. the ultra-low ($< 1.0 \times 10^4$), low ($1.0 \times 10^4 \sim 3.0 \times 10^5$), moderate ($3.0 \times 10^5 \sim 5.0 \times 10^6$) and high Re_c ($> 5.0 \times 10^6$), are proposed based on their characteristics of the C_L-Re_c relationship and the flow structure. It has been observed that T_u has a more pronounced effect at lower Re_c than at higher Re_c on the shear layer separation, reattachment, transition, and formation of the separation bubble. As a result, C_L, C_D, C_L/C_D and their dependence on the airfoil angle of attack all vary with T_u. So does the critical Reynolds number $Re_{c,\mathrm{cr}}$ that divides the ultra-low and low Re_c regimes. It is further noted that the effect of increasing T_u bears similarity in many aspects to that of increasing Re_c, albeit with differences. The concept of the effective Reynolds number $Re_{c,\mathrm{eff}}$ advocated for the moderate and high Re_c regimes is re-evaluated for the low and ultra-low Re_c regimes. The $Re_{c,\mathrm{eff}}$ treats the non-zero T_u effect as an addition of Re_c and is determined based on the presently defined $Re_{c,\mathrm{cr}}$. It has been found that all the maximum lift data from both present measurements and previous reports collapses into a single curve in the low and ultra-low Re_c regimes if scaled with $Re_{c,\mathrm{eff}}$.

PUBLICATIONS ARISING FROM THE THESIS

1. **Wang S.**, Zhou Y., Alam M.M. and Yang H.X., "Effect of turbulence intensity on the low Reynolds number airfoil wake," The Proceedings of The 4th International Conference on Jets, Wakes and Separated Flows (ICWJF2013), 17-21 September, Nagoya, Japan, ICJWSF2013-1225 (2013).
2. **S. Wang**, Y. Zhou, M. M. Alam, and H. X. Yang, "Turbulent Intensity Effect on Low Reynolds Number Airfoil Wake," Fluid-Structure-Sound Interactions and Control, Lecture Notes in Mechanical Engineering, Y. Zhou et al. (eds.), Springer-Verlag Berlin Heidelberg (2014)
3. **Shu Wang**, Yu Zhou, and Md.Mahbub Alam, "Effects of Reynolds Number and Turbulent Intensity on a Low Reynolds Number Airfoil," 32nd AIAA Applied Aerodynamics Conference, 15-20 June, Atlanta, GA, AIAA 2014-2018 (2014)
4. **S. Wang**, Y. Zhou, Md. Mahbub Alam, and H. Yang, "Turbulent intensity and Reynolds number effects on an airfoil at low Reynolds numbers," Physics of Fluids 26, 115107 (2014); http://dx.doi.org/10.1063/1.4901969

ACKNOWLEDGEMENTS

I would like to express my appreciation to my supervisor Dr. LIU Yang for helping me to finish this unforgettable experience in The Hong Kong Polytechnic University.

I also would like to thank Professor WEN Chih-yung, my classmates Dr. ZHANG Pei and Dr. ZHANG Bingfu, for many useful discussions and a lot of help.

I am very grateful to my parents Mr.WANG Peiyu and Mrs. WANG Guangling, my sister LI Qingsu, my wife Mrs. ZHANG Siyuan and my son WANG Xirui. Their love are always around me for these years. I could not manage to complete this thesis without their support.

CONTENTS

LOW REYNOLDS NUMBER AIRFOIL AERODYNAMICS

CHAPTER I. INTRODUCTION

Investigations on the aerodynamics of airfoil are traditionally driven by the need of aeronautical applications and are focused on the flow of small angle of attack (α), i.e. the pre-stalled condition, and the chord Reynolds number $Re_c \equiv U_\infty c/\nu$ is largely over 5×10^5, where U_∞ is the free-stream velocity, c the airfoil chord length and ν the fluid kinematic viscosity. The knowledge obtained is now inadequate due to developments in small wind turbines, small unmanned aerial vehicles (UAVs) such as micro air vehicles (MAVs), nano air vehicles (NAVs), and increasing interests in understanding bird and insect flights.[1-3] All these activities involve very low Re_c. For instance, the Re_c is commonly less than 2×10^5 for MAVs,[4] less than 1.5×10^4 for NAVs,[5] and even lower for insect flights.[6] In the study of the airfoil wake, $Re_c \lesssim 5 \times 10^5$ is often called the low Reynolds number because of the occurrence of reattachment after laminar separation, which forms the so-called laminar separation bubble (LSB).[7] At $Re_c < 1 \times 10^4$, the separated boundary layer is characterized by a delayed transition and remains laminar for a rather long longitudinal distance, not prone to reattachment, implying the absence of the LSB or a qualitative change in the flow structure.[8] It is well known that an airfoil may stall given an adequately large α, which is associated with the burst of the separation bubble and a rapid drop in the lift coefficient C_L for a small increase in α. However, at $Re_c < 1 \times 10^4$, the typical feature of stall — the rapid drop in C_L does not occur due to the absence of the separation bubble,[9] which is referred to as the ultra-low Reynolds number.[8, 10]

Developments in small wind turbines may involve not only small Re_c but also large α. At the starting stage of small wind turbines, Re_c increases from 10^4 to 10^5 and α may change over the range of 0° ~ 90°. Furthermore, the turbulence level T_u ($\equiv u'_{\mathrm{rms}}/\overline{U}$) of wind often varies from time to time, where overbar and subscript rms denote the local mean and root mean square values of the instantaneous streamwise velocity U and its fluctuating component u', respectively. For example, in coastal or typhoon-affected areas, wind turbine blades may be under strongly turbulent high winds. Naturally, there is a strong need to understand the effect of T_u on the low Re_c airfoil at a large α.

The effect of T_u on airfoil aerodynamics has received considerable attention in the literature for the low-to-high Re_c range; this effect is largely associated with the stall, increasing the stall angle or the maximum C_L.[11-14] Hoffmann[12] measured C_L and drag coefficient C_D of NACA 0015 airfoil at $Re_c = 2.5 \times 10^5$. He found that a variation in T_u from 0.25 % to 9.0 % resulted in an increase in the maximum of C_L by 30 %. Similar conclusions were made experimentally by Mish and Devenpor[13] and numerically by Gilling *et al.*[14] for NACA 0015 airfoils at $Re_c = 1.17 \times 10^6$ and 1.6×10^6, respectively. Huang and Lee[15] investigated the T_u effect on both aerodynamic loads and surface-flow characteristics of the NACA 0012 airfoil at $Re_c = 0.5 \times 10^5$ to 1.5×10^5, with T_u varying between 0.20 % and 0.65 %. It was found that an increase in T_u at $T_u < 0.45$ % could effectively delay the stall. The effect of T_u on the maximum C_L became significant for $T_u >$ 0.45 %. Investigations on other airfoils, such as NACA 65_4-421 and HQ 17,[16, 17] showed a similar dependence on T_u.

One may question whether the previously obtained knowledge of the T_u effect on flow at $Re_c > 0.5 \times 10^5$ could be extrapolated to the low- and ultra-low Re_c flow, i.e. $Re_c < 0.5 \times 10^5$. This extrapolation is naturally not recommendable in view of the difference, discussed above, in the flow structure about the airfoil between the regimes of high-, low-and ultra-low Re_c. This work aims to investigate experimentally the T_u effect on the aerodynamics of a NACA 0012 airfoil at low- and ultra-low Re_c. Three levels of T_u, i.e. 0.6 %, 2.6 % and 6.0 %, have been examined over $\alpha = 0° \sim 25°$ for $Re_c = 5.3 \times 10^3$ and 2.0×10^4, which represent the ultra-low- and low-Re_c regimes, respectively. Experimental details are given in Sec. II. Results are presented and discussed in detail in Secs. III-V. This work is concluded in Sec. VI.

CHAPTER II. EXPERIMENTAL DETAILS

A. Water tunnel, test model and turbulence generator

Experiments were performed in a closed-loop water tunnel, with a test section of 0.3 m (width) × 0.6 m (height) × 2.4 m (length). The water speed in the test section ranges from 0.05 to 4 m s^{-1}. The flow non-uniformity is less than 0.1 %. The tunnel was described in detail by Wang *et al.*[18]. A NACA 0012 airfoil, with a span length of s = 0.27 m and c = 0.1 m, was used as the test model and mounted horizontally in the test section. The angle of attack was adjustable by rotating the airfoil supporting shaft, 0.4 c away from the leading edge (Figure II-1 a), with a maximum uncertainty of 0.5 degree. One endplate was mounted on each side of the model to minimize the end effect (Figure II-1 c). Measurements were conducted at free-stream velocity U_∞ = 0.053 and 0.200 ms^{-1}, corresponding to $Re_c = 5.3 \times 10^3$ and 2.0×10^4, respectively. At these speeds, T_u was measured to be about 0.6 %.

The higher T_u was achieved by placing a grid upstream of the airfoil model. The characteristic dimensions of the grid are M = 40 mm, D = 10 mm and H = 40 mm, with a porosity of 64 % (Figure II-1b). The grid was installed at the end of the tunnel contraction section, generating the closely uniform and isotropic turbulence.[15, 19] Laser Doppler anemometer (LDA) was used to measure the flow velocity with flow seeded with the polyamide particles of 20 μm in diameter. The LDA measurement accuracy depends on seeding particles, and is adversely influenced by impurities that are inevitably present in natural water. At present low flow speeds, this accuracy is adequate for measuring the mean velocity but not for the fluctuating velocity. As such, an LDA-calibrated hot-film probe, sensitive to velocity fluctuation, was used to measure T_u. The measurement uncertainties of both mean and fluctuating velocities are estimated to be within 1 % based on 10 repeated tests.

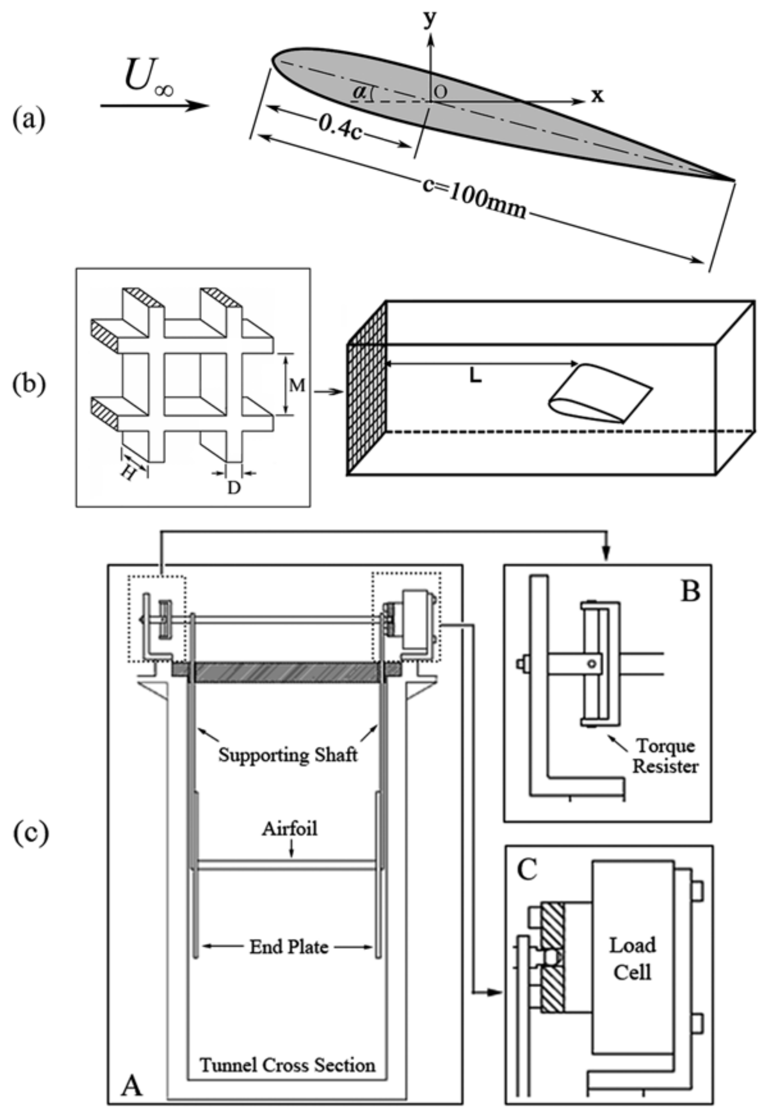

Figure II-1. (a) Airfoil model and definition of the coordinate system; (b) schematic of grid and airfoil installation in the water tunnel; (c) setup of force measurement: (A) cross-sectional view, (B) torque resister, (C) load cell

A variation in T_u was achieved by changing distance L from the grid to the airfoil model (Figure II-1 b). The choice of L is based on two considerations, i.e. the uniformity of $\overline{U}$ and suitable T_u. U was measured using LDA at a number of points along the z direction in the y-z plane to estimate the uniformity of $\overline{U}$ and T_u. As shown in Figure II-2 (a), there is discernible variation in $\overline{U}$ across flow at L = 10M but not so at L = 14M. A parameter I_u ($\equiv u''_{\mathrm{rms}} / <\overline{U}>$) is defined to quantify the departure from the perfect uniformity, where $<\overline{U}>$ represents the averaged $\overline{U}$ across flow and u'' is the variation of $\overline{U}$ about the average. Both T_u and I_u decay with increasing L, following a power law (Fig. 2 b). Three free-stream turbulence levels, i.e. T_u = 6.0 %, 2.6 % and 0.6 %, of the flow (table I) were obtained at L = 14M and 41M and removing the turbulence generator, respectively, all with I_u less than 1 %. According to table 1, $u'_{\mathrm{rms}}/v'_{\mathrm{rms}}$ was less than 1.2, showing a quasi-isotropic freestream turbulence for all the three T_u levels, where v' is the fluctuation component of the lateral instantaneous velocity. Based on the Taylor hypothesis, the streamwise integral length scales L_u^x could be estimated by $L_u^x = \overline{U}\int_0^{\tau_0} R_u(\tau)d\tau$, where R_u is the autocorrelation functions of single point temporal fluctuating streamwise velocity, τ is the time difference and τ_0 is where R_u equals the first zero. L_u^x was 0.16c and 0.25c at T_u = 6.0 % and 2.6 %, respectively. The L_u^x of the order of magnitude of c means that the inflow conditions are steady and the flow is turbulent on the airfoil.[20] Figure 3 presents the power spectrum of streamwise velocity in the freestream. The magnitude of the power spectrum increases with T_u for all frequencies and no prominent peak can be seen, irrespective of the T_u level, ensuring the airfoil not affected by fluctuations at a particular frequency.

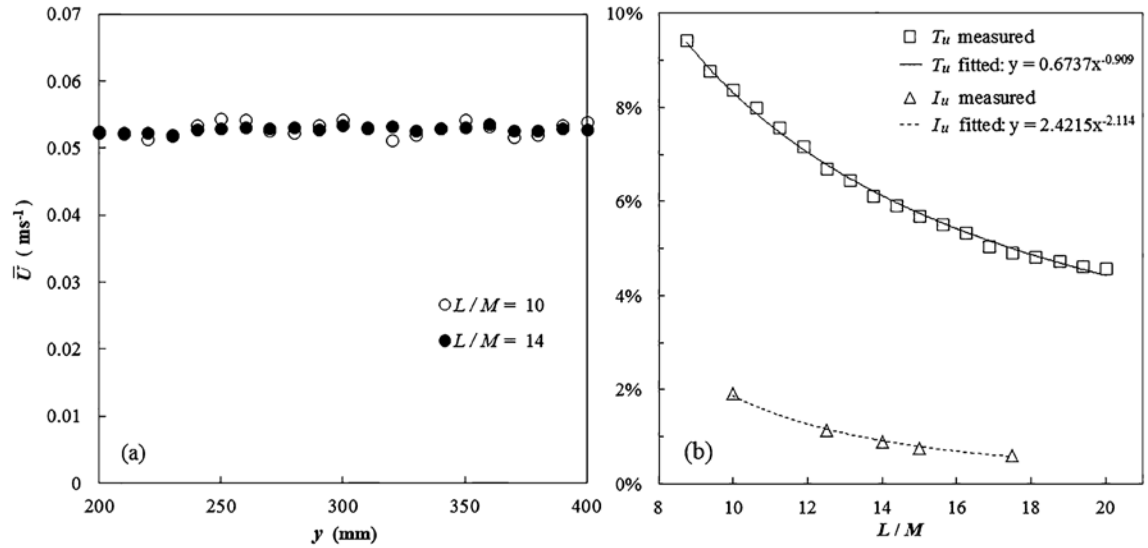

Figure II-2. (a) The distribution of $\overline{U}$ at L/M = 10 and 14; (b) dependence of streamwise turbulence intensity T_u and inhomogeneity I_u ($\equiv u''_{\mathrm{rms}} / <\overline{U}>$) on L/M.

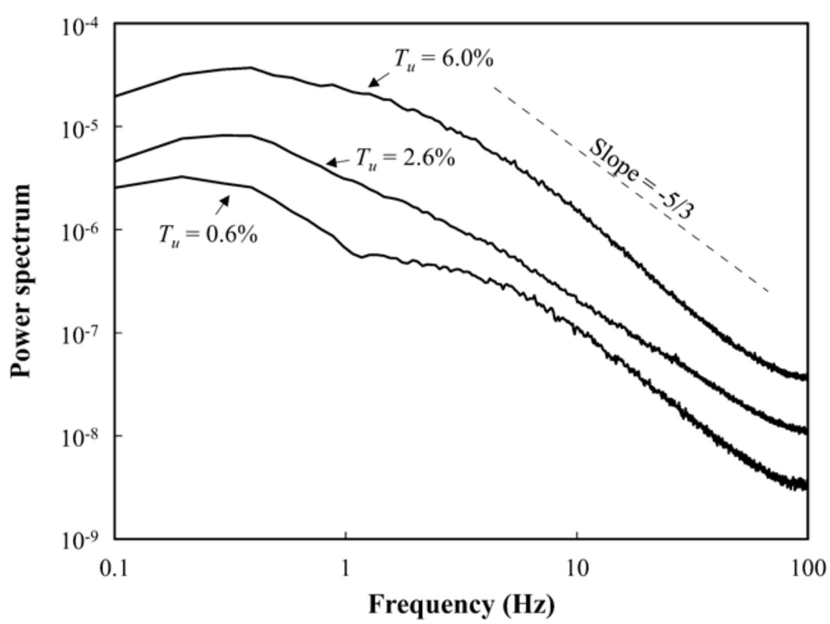

Figure II-3. Power spectrum of freestream streamwise velocity for different T_u.

Table II-I. Characteristics of the free-stream flow.

No.	Grid	L / M [a]	I_u (%) [b]	T_u (%) [c]	u'_{rms} / v'_{rms} [d]	L_u^x / c [e]
1	No	-	0.26	0.6	1.06	-
2	Yes	41	0.35	2.6	1.22	0.25
3	Yes	14	0.90	6.0	1.18	0.16

[a] L is the downstream distance of airfoil model from the gird and M is the grid mesh size.
[b] I_u is the uniformity of the free-stream flow.
[c] T_u is the turbulence intensity of the free-stream flow.
[d] u'_{rms} and v'_{rms} are the rms of the fluctuation components of intantanous streamwise and lateral velocity respectively.
[e] L_u^x is the streamwise integral length scale of of the free-stream flow.

B. Force measurements

Figure 1(c) shows the setup of the force measurement system, which was modified from that of Alam *et al.*[8] to accommodate a new load cell model of higher resolution. The fluid force on the airfoil and its endplates was transmitted to the load cell installed above water via the supporting shaft, as shown in part A. The force resulted in a torque, influencing the output of the load cell. To minimize this influence, a torque-resistor, marked by part B, was deployed, which was fixed at one connection pole. The end of the connection pole on the load cell side could freely rotate relatively to the cell, marked by part C, thus allowing the force to be transmitted to the cell but not the torque. One calibrated Kyowa WGA-800c load cell with a measuring range of ±10N was used to measure the lift and drag forces, F_L and F_D. The lift and drag coefficients are calculated by

$$C_L = \frac{F_L}{\frac{1}{2}\rho U_\infty^2 cs}, \quad (1)$$

$$C_D = \frac{F_D}{\frac{1}{2}\rho U_\infty^2 cs}, \quad (2)$$

where ρ is the fluid density. The measured force signals were amplified and low-pass-filtered at the cutoff frequency of 10 Hz before being sampled at 30 Hz through an A/D board. The sampling duration was 5 minutes. The resolution of the load cell is within 0.002 N, resulting in the uncertainties of less than 5% in the estimate of C_D and C_L. For $\alpha = 0° \sim 25°$, the blockage ratio of the airfoil ranges from 2 % to 7.8 %. Correction is made for both C_L and C_D for all angles, following Maskell[21] and Barlow *et al.*[22]. Since the correction tends to fail for a blockage of higher than 6%,[22] additional error may occur in both C_L and C_D at $\alpha > 20°$. As a result, present C_L and C_D at $\alpha = 25°$ tend to be larger than the actual value in the absence of blockage. No further correction is attempted due to a lack of reliable methods. Indeed, $\alpha > 20°$ is well beyond the stall, which is not the focus of the present investigation.

C. LIF flow visualization

A laser induced fluorescent (LIF) flow visualization system was used to visualize the airfoil wake at $Re_c = 5.3 \times 10^3$ in the *x*-*y* plane through the airfoil mid-span, that is thought to be representative of the whole span, as the endplates installed made the flow two dimensional.[8, 23] A pin hole of 1.0 mm in diameter was drilled at the airfoil leading edge for the release of dye (Rhodamine 6G 99 %). The flow marker or dye was stored in a small tank placed at about 1 m above the airfoil. The tank was connected to the airfoil via a rubber tube. A regulator valve was used to control the flow rate of dye. A laser beam from a 6W argon ion laser source (Spectra Physics) was transmitted through an optic fibre and transformed into a plane sheet using a laser-sheet probe. The visualized flow images were recorded using a Sony video camera (DCR-PC100E) with a framing rate of 25 frames per second.

D. PIV measurements

A Dantec particle image velocimetry (PIV) system (PIV2100) was used to measure flow in the *x*-*y* plane at mid-span of the airfoil (Fig. 1 a). The airfoil was made of transparent Plexiglas, allowing the flow field of interest to be visualized without shadow except a passage for dye injection. The same flow seeding as in the LDA measurements was used. The PIV image size was 2048 × 2048 pixels, covering an area of 226 mm × 226 mm. In image processing, an interrogation window of 8 × 8 pixels was used with 50 % overlap in each direction. The ensuing in-plane velocity fields consisted of 511 × 511 vectors. The number of erroneous vectors in the captured flow field was about 443, corresponding to 0.17 % of the total. These erroneous vectors occur due to insufficient light intensity in the shadow of the dye injection passage built in the airfoil model. The moving-average validation built in the data processing software of Dantec PIV was used to reject erroneous vectors. The rejected vectors were replaced by vectors interpolated from surrounding vectors. See Host-Madsen and McCluskey[24] for more details. About 450 images with good convergence were captured for each test case to estimate the iso-contours of $\overline{U}$.

CHAPTER III. REYNOLDS NUMBER EFFECT

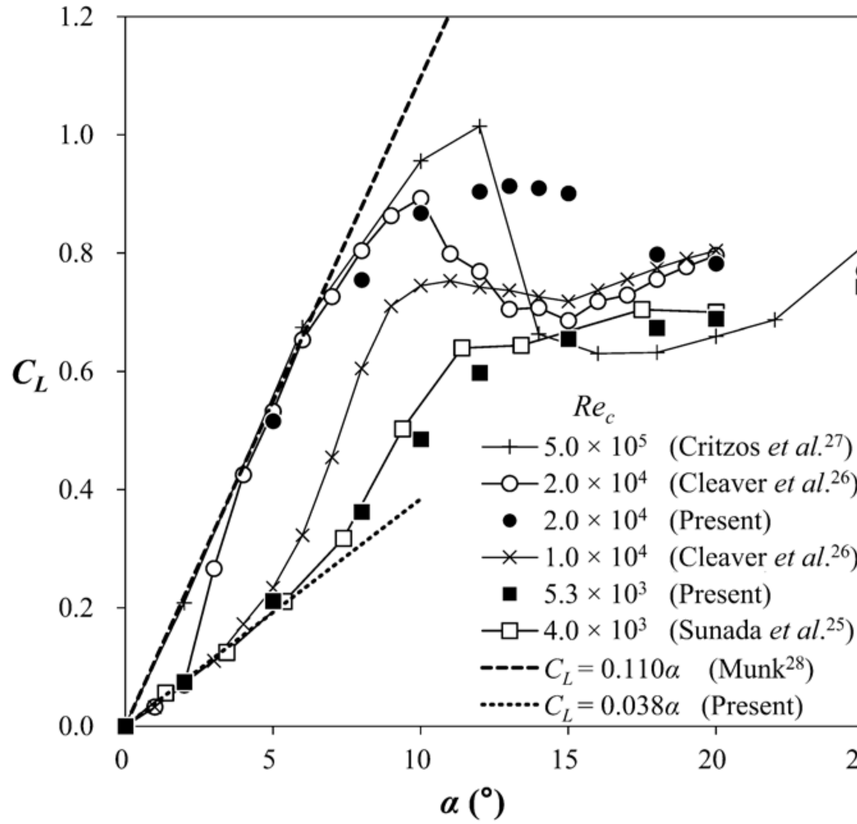

Figure III-1. Comparison in C_L between present and previous measurements for NACA 0012.

The measured C_L at T_u = 0.6 % is compared with the published data for $Re_c = 4.0 \times 10^3 \sim 5.0 \times 10^5$ in Figure III-1. All the data has a T_u value of ⩽ 1 % and flow is nominally two-dimensional. The present results are in general in good agreement with those of comparable Re_c. All the C_L data at $Re_c = 1.0 \times 10^4$ or more exhibit a rise-and-fall behaviour, i.e. the occurrence of stall. The present C_L at $Re_c = 5.3 \times 10^3$ however does not show the rise-and-fall behaviour, which is refered here and after as the absence of stall, as noted by Sunada *et al.*[25] at $Re_c = 4.0 \times 10^3$. A similar observation was also reported by Alam *et al.*[8]. The present C_L at $Re_c = 2.0 \times 10^4$ agrees well before the stall angle with Cleaver *et al.*[26] at the same Re_c. However, there is a discrepancy in α for the occurrence of the stall, at least partially due to a lower T_u (< 0.5 %) in measurement of Cleaver *et al.*[26]. A lower T_u corresponds to a smaller stall angle.[11-14] Furthermore, their measurement had a blockage ratio of more than 6% for $\alpha > 13°$, but no information was given on whether the data was corrected, which should also contribute to the discrepancy. Two more sets of the C_L data, i.e. $Re_c = 1.0 \times 10^4$ from Cleaver *et al.*[26] and 5.0×10^5 from Critzos *et al.*[27], are included in Figure III-1 to facilitate the discussion on the influence of Re_c on the C_L variation with α.

A. Dependence of C_L on α and underlying flow physics

The C_L dependence on α exhibits a marked change in slope with Re_c varying. For $Re_c = 5.0 \times 10^5$, C_L increases linearly from $\alpha = 0$ to 6° with an initial slope of 0.110 (or 2π if radian is used as unit of α), as predicted theoretically based on inviscid thin airfoil theory.[28] As Re_c is reduced to 2.0×10^4, C_L shows a different initial slope of about 0.038 from α = 0 to 2° but then recovers rapidly in a nonlinear manner. This nonlinear variation at small α was observed by Panda and Zaman[29] and by Laitone[30] for NACA 0012 at $Re_c = 2.0 \sim 4.0 \times 10^4$ and by Lutz *et al.*[31] for NACA 0009 at $Re_c = 5.0 \times 10^4$. As flow visualization photographs (Figure III-2 a, b) indicate, the boundary layer over the airfoil with $\alpha = 0 \sim 2°$ is laminar at $Re_c = 2.0 \times 10^4$, and flow separation occurs near the trailing edge on the suction side of airfoil, without reattachment. On the other hand, the separated flow reattaches at $\alpha > 2°$, producing a separation LSB, as illustrated in Figure III-2 (c). More details of the separation bubble, enclosed by the contour of $\overline{U}^* = 0$ and the airfoil surface, for the same α are evident from the iso-contours of the PIV-measured $\overline{U}^*$ (Figure III-2 d). Asterisk denotes normalization by c and/or U_∞ in this paper. Note that the transition in the shear layer occurs prior to reattachment (Figure III-2 c). Correspondingly, $dC_L/d\alpha$ reduces from α = 3 to 9°, where the transition takes place between flow separation and reattachment. In the absence of reattachment (α > 9°), $dC_L/d\alpha$ drops to a negative value and then increases. These observations implies that a simplified correlation of $dC_L/d\alpha$ and its underlying flow state could be found when taking the nonlinear C_L dependence on α as piecewise linear segments.

A lower Re_c (= 1.0×10^4) enables the initial linear range to be extended to α = 3°, and then incurs a recovery in C_L up to α = 10°, which is associated with an increasing slope from α = 3 to 7° but then decreasing up to α = 10°, that is, α = 7° is the inflection point. The separation bubble is formed in both ranges of α, though exhibiting distinct features. At α = 3 ~ 7°, the shear layer transition occurs after reattachment; as such, the bubble is long and laminar, all the way from separation to reattachment. On the other hand, at α = 7 ~ 10°, the transition takes place between flow separation and reattachment; the bubble is shorter and partially laminar, that is, laminar separation followed by turbulent reattachment. Apparently, the inflection point α = 7° is a turning point, where the transition occurs at reattachment. As noted in the previous paragraph, at Re_c = 2.0×10^4, the bubble where the transition occurs before reattachment corresponds to reducing $dC_L/d\alpha$ from α = 3 to 9°. It may be inferred that the starting α for this bubble type is larger at smaller Re_c (α = 3° at Re_c = 2.0×10^4; α = 7° at Re_c = 1.0×10^4), in agreement with our intuition.

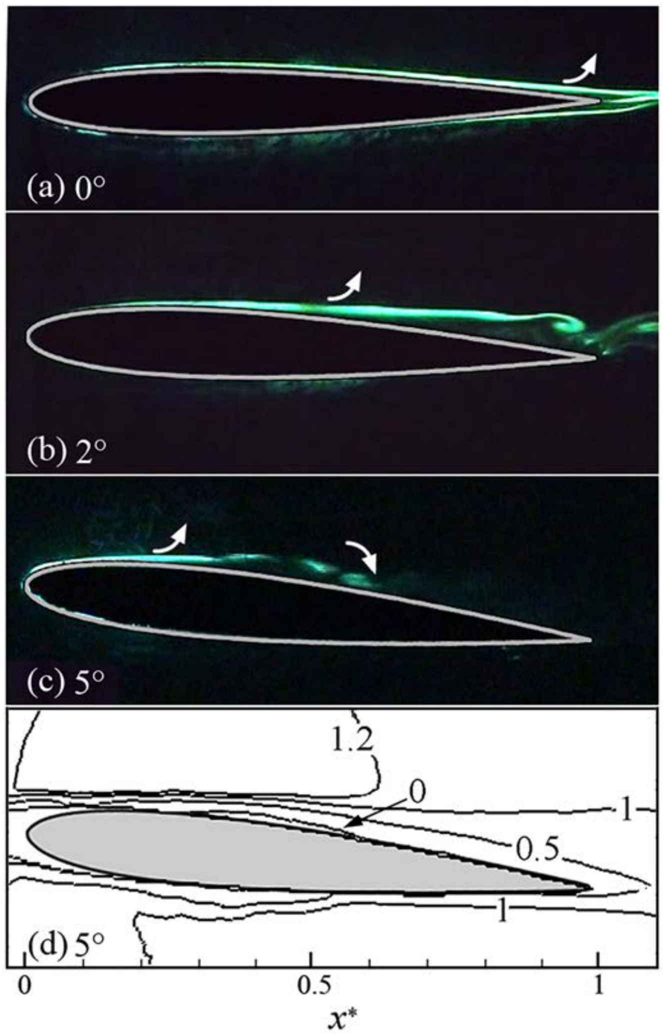

Figure III-2. Typical photographs captured in LIF flow visualization: (a) $\alpha = 0°$, (b) 2°, (c) 5°, (d) the iso-contours of PIV-measured $\overline{U}^*$ ($\alpha = 5°$). $Re_c = 2.0 \times 10^4$. Symbols ↗ and ↘ indicates the occurrence of flow separation and reattachment, respectively.

As Re_c decreases to 5.3×10^3 and 4.0×10^3, the initial linear range of C_L versus α is extended further to $\alpha = 5°$, and then C_L varies almost linearly up to $\alpha = 12°$ with a larger slope. In both α ranges, the separated flow does not reattach. The different slopes are linked to the fact that the shear layer is elongated, rolling up behind the trailing edge, in the former but rolls up over the airfoil surface in the latter (Figure III-3), with rolling up position moving upstream with α. The drastic drop in C_L does not crop up in the remaining

α examined, implying the absence of stall and the absence of reattachment of the separated flow over the entire α range examined. The above observations are confirmed by flow visualization data. Typical photographs (Figure III-3) show that the separation point shifts gradually towards the leading edge without flow reattachment from $\alpha = 0$ to 20°**.** In this α range, the recovery of C_L towards the theoretical 0.110α is due to (i) boundary layer separation shifted toward the leading edge, (ii) upstream shift of shear-layer rollup, and (iii) transition of the shear-layer/wake from laminar to turbulent shifted toward the separation point. While point (i) makes a predominant contribution to increasing lift for $\alpha \leqslant 5°$, points (ii) and (iii) produce additional contribution for lift increase over $5° < \alpha \leqslant 12°$. However, all these mechanisms are feeble for $\alpha > 12°$. The curve therefore displays a turning point at $\alpha \approx 12°$ after which the increase in C_L is slowed down with increasing α. The observation is rather similar to that found for inclined plates at $Re_c = 4.0 \times 10^3$ by Sunada *et al.*[25].

In summary, the C_L dependence on α up to the pre-stall is characterized at $Re_c = 2.0 \times 10^4$ by two distinct behaviours, (i) a constant $dC_L/d\alpha$ (= 0.038) at small α, associated with laminar flow separation without reattachment, and (ii) a decreasing $dC_L/d\alpha$ at larger α linked to laminar flow separation followed by turbulent reattachment. At $Re_c = 1.0 \times 10^4$, other than behaviours (i) and (ii), the C_L dependence displays one more distinct behaviour, that is, (iii) an increasing $dC_L/d\alpha$ due to laminar separation followed by laminar reattachment at $\alpha = 3 \sim 7°$. With decreasing Re_c, the α range over which behaviour (i) occurs is enlarged and that corresponding to (ii) shrinks. By $Re_c \approx 5.3 \times 10^3$ or lower, the C_L dependence consists of two linear variations connected to shear layer rollup behind the trailing edge and over the surface, respectively.

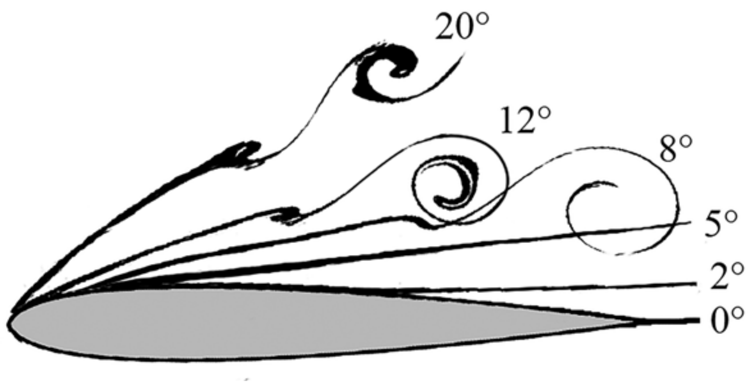

Figure III-3. Instantaneous separated shear layers at different α (extracted from LIF flow visualization photographs). $Re_c = 5.3 \times 10^3$.

B. Classification of the Re_c regimes

A significant Re_c effect on C_L is also reflected in a variation in the maximum C_L, i.e. $C_{L,\max}$. The $C_{L,\max}$ is an important parameter in terms of the performance of an airfoil. It has been well established that $C_{L,\max}$ strongly depends on Re_c for large Re_c.[23, 32-34] Figure III-4 presents a collection of $C_{L,\max}$ of NACA 0012 for a wide range of Re_c in the literature [25, 26, 35-39] as well as the present measurement. In the absence of stall, C_L will reach its global maximum at $\alpha \approx 40°$.[8] However, in order to compare the lift performance within stall α range, $C_{L,\max}$ is defined in such case as the point at which C_L/α reaches maximum. C_L increases very slowly with α after this turning point. The dependence of $C_{L,\max}$ on Re_c from McCroskey[23] is given to cover the moderate and high Re_c range. A relatively large scattering is expected over the low Re_c range because of different experimental conditions. In general, $C_{L,\max}$ grows with increasing Re_c. However, the increasing rate can be very different for different Re_c ranges. As such, four Reynolds number regimes may be identified in terms of the dependence of $C_{L,\max}$ on Re_c, each associated with distinct flow physics behind.

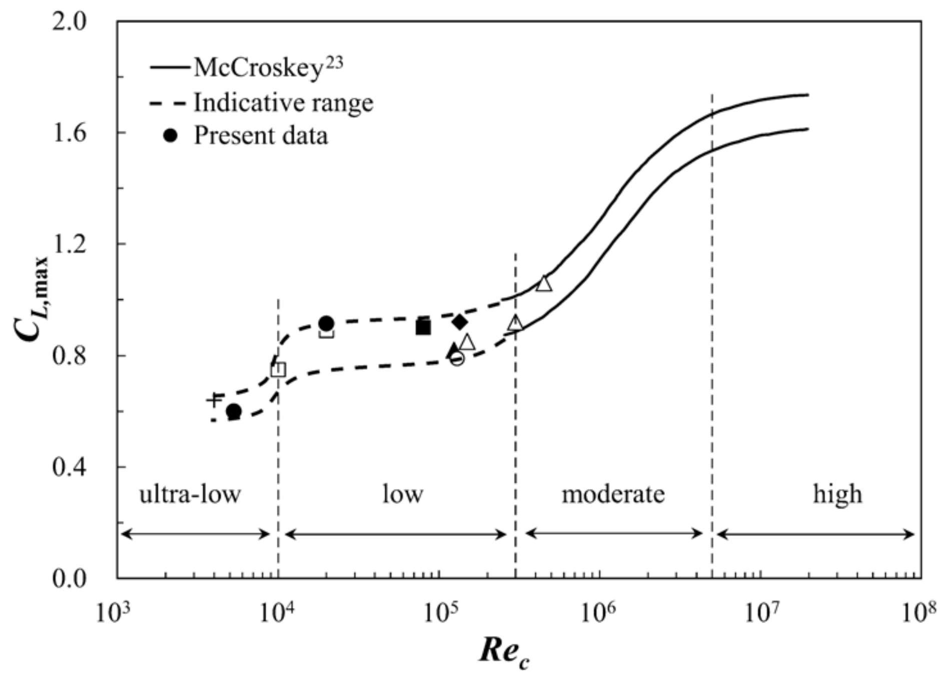

Figure III-4. Dependence of $C_{L,\max}$ on Re_c of NACA 0012 airfoil: +Sunada *et al.*[25]; ■ Chen and Choa[35]; □ Cleaver *et al.*[26]; ○ Grager *et al.*[36]; ◆ Lee and Gerontakos[37]; ▲ Wong and Kontis[38]; △ Sant and Ayuso[39].

The ultra-low Reynolds number regime refers to $Re_c < 1 \times 10^4$. The term the ultra-low Reynolds number was first used by Kunz and Kroo[10] and then by Alam *et al.*[8] and Zhou *et al.*[9]. In this Re_c range, $C_{L,\max}$ is small, about 0.6; the boundary layer is laminar and separates at small α, e.g. $\alpha < 2°$ for $Re_c = 5.3 \times 10^3$. The separated shear layer remains laminar for a prolonged distance without reattachment and hence without any separation bubble formed. As a result, stall is absent. With an increase in α, an enhancement in C_L results mainly from a shift in the shear layer separation and rollup toward the leading edge and a shift in transition from laminar shear layer to turbulent on the suction side toward the separation point. All the shifts make positive contribution to C_L, though the separation point change contributes predominantly at $\alpha \leqslant 5°$ and the other two at $\alpha > 5°$. Thus, the $C_{L.\max}$ variation is determined by the combined effects of the three phenomena.

In the low Reynolds number regime from $Re_c = 1.0 \times 10^4$ to 3.0×10^5, $C_{L,\max}$ exhibits a weak dependence on Re_c, increasing slowly from around 0.8 to 1.0, and the shear layer may reattach on the airfoil surface, forming a separation bubble.[8] The shear layer transition occurs near reattachment, specifically, after reattachment for small α and before for large α, as discussed above. The bubble size is prolonged because transition takes place near the reattachment point. The $C_{L,\max}$ is limited by a thin-airfoil stall, i.e. stall type III, where the bubble bursts.[33, 40]

The moderate Reynolds number regime covers $Re_c = 3.0 \times 10^5 \sim 5.0 \times 10^6$. For α near the stall, the shear layer transition occurs between the separation and reattachment points. With increasing Re_c, the transition shifts toward the separation point and the separation bubble is shortened. As a result, $C_{L,\max}$ increases rather rapidly, from around 1.0 at $Re_c = 3.0 \times 10^5$ to 1.6 at $Re_c = 5.0 \times 10^6$. The $C_{L,\max}$ is limited by a leading-edge stall or stall type II, with abrupt flow separation near the leading edge and in general without subsequent reattachment.[33, 40]

In the high Reynolds number regime, viz. $Re_c > 5 \times 10^6$, $C_{L,\max}$ displays a weak dependence on Re_c again and is almost a constant of around 1.6. Transition occurs now in the boundary layer prior to separation. An increase in Re_c results in a shift in the boundary layer transition toward the forward stagnation point. $C_{L,\max}$ is less sensitive to Re_c in the absence of a LSB and is limited by a trailing-edge stall, i.e. stall type I.[33, 40] The turbulent separation point moves from the trailing to leading edge as α increases.

C. Flow structure around airfoil

Flow around the airfoil may exhibit different structures with increasing α in each Re_c regime. Eight distinct flow structures have been identified on the suction side of the airfoil, viz.

A Fully attached laminar boundary layer；

B Partially attached laminar boundary layer which separates near the trailing edge and then rolls up and/or experiences transition further downstream;

C Fully separated laminar shear layer near the leading edge with a subsequent transition downstream but without reattachment;

D Laminar bubble, i.e. laminar flow from separation to reattachment;

E Partially laminar bubble, where laminar separation is followed by turbulent reattachment;

F Fully attached turbulent boundary layer;

G Trailing-edge separated turbulent boundary layer, where flow separation occurs near the trailing edge;

H Fully separated turbulent shear layer where flow separation occurs near the leading edge.

Figure III-5 shows schematically these flow structures and the sequence of the flow structures and stall types that occur as α increases in each Re_c regime, that is, A→B→C in the ultra-low Re_c regime, B→D→ E→stall type III→C in the low Re_c regime, E→ stall type II→C in the moderate Re_c, and F→G →stall type I→H in the high Re_c regime.

These flow structures and their dependence on Re_c and α indicate that shear layer transition, separation and reattachment determine crucially the behaviour of the airfoil wake. In a flow over forward facing steps, Chapman *et al.*[41] concluded that the variable most important to a separated flow is the location of transition relative to reattachment and separation positions.They classified the separated flows into three essentially different types, depending on the relative location of transition: a “pure laminar” type for which transition is downstream of reattachment, a “transitional” type for which transition is between separation and reattachment, and a “turbulent” type for which transition is upstream of separation. Similarly, the occurrence sequence of transition, separation and reattachment determine the flow regimes of the airfoil wake. At very small α and Re_c, the laminar boundary layer does not separate from the airfoil, engendering flow structure A, e.g. at $\alpha = 0°$ in Figure III-3. With α and/or Re_c increased, the boundary layer separates before the trailing edge and rolls up behind the trailing edge (e.g. at $\alpha = 2$ and 5° in Figure III-3), that is, flow structure B prevails, causing a linear increase in C_L with a smaller slope (Figure III-1, $Re_c = 5.3 \times 10^3$). When α is large enough, the shear layer separates near the leading edge and rolls up over the surface without reattachment (flow structure C). This may cause C_L to increase almost linearly or to deteriorate, as illustrated for $\alpha > 5°$ in the ultra-low Re_c regime ($Re_c = 5.3 \times 10^3$) and for $\alpha > 10°$ in the low and moderate Re_c regimes ($Re_c = 2.0 \times 10^4$), respectively. Laminar reattachment is possible at small α, with transition taking place after reattachment, leading to flow structure D responsible for increasing $dC_L/d\alpha$ from $\alpha = 3$ to 7° at $Re_c = 1.0 \times 10^4$. Further increase in α and/or Re_c causes transition before reattachment (Figure III-2c) or flow structure E, corresponding to a decreasing $dC_L/d\alpha$. See Figure III-1 for $Re_c = 1.0 \times 10^4$ and $7° < \alpha < 10°$ or $Re_c = 2.0 \times 10^4$ and $\alpha = 3 \sim 9°$. If transition occurs before separation, the airfoil is surrounded completely (flow structure F) or partially (flow structure G) by turbulent boundary layer. The latter is associated with the best aerodynamic performance, e.g. achieving the highest $C_{L,\max}$ in the high Re_c regime. A slight increase in α, compared with flow structure G, causes turbulent boundary layer separation very near the leading edge or flow structure H.

Re_c plays a crucial role in determining the sequence of shear layer transition, separation and reattachment. As is well known, given a flow, Re_c is the determining parameter for the transition of the boundary layer. A higher Re_c tends to promote the shear layer transition. For example, the shear layer starts to roll up and transits near the trailing edge at $\alpha = 2°$ for $Re_c = 2.0 \times 10^4$ (Figure III-2b). On the other hand, the shear layer remains laminar and there is no sign of transition before the trailing edge at the same α for $Re_c = 5.3 \times 10^3$ (Figure III-3). The higher Re_c also promotes flow separation. At $\alpha = 0°$, flow separation occurs on both sides of airfoil at $x^* = 0.9$ for $Re_c = 2.0 \times 10^4$ (Figure III-2a) but remains attached for $Re_c = 5.3 \times 10^3$. At $\alpha = 2°$, the separation point occurs at $x^* = 0.48$ for $Re_c = 2.0 \times 10^4$ (Figure III-2b) but at $x^* = 0.6$ for $Re_c = 5.3 \times 10^3$. Similar observations were made both experimentally by Boutilier and Yarusevych[42] and numerically by Kunz and Kroo[10]. As a result of the Re_c effects on separation, transition and reattachment, the flow structure change at a given pre-stall α follows the sequence of A → B → (D, E) → (F, G) with increasing Re_c, as shown in Figure III-5.

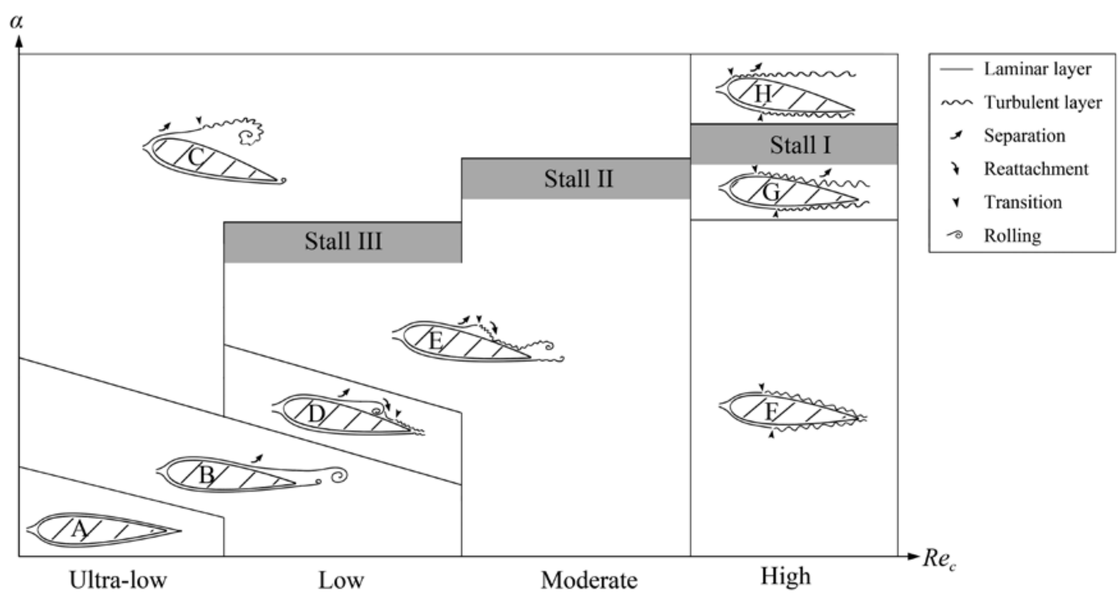

Figure III-5. Schematic of flow structures around airfoil for each Re_c regime.

CHAPTER IV. TURBULENT INTENSITY EFFECT

A. Mean lift, drag and lift-to-drag ratio

The turbulence level T_u has a significant effect on C_L, C_D and C_L/C_D in the ultra-low Re_c regime. Figure IV-1 presents the C_L, C_D and C_L/C_D variations with α ($\leq 30°$) at $Re_c = 5.3 \times 10^3$. At $T_u = 0.6$ %, C_L increases monotonically with α, that is, no separation bubble and hence no stall occurs. At $T_u = 2.6$ %, C_L exceeds that at $T_u = 0.6$ % over $\alpha = 2 \sim 25°$ and shows a rather sharp peak at $\alpha \approx 12°$, suggesting the formation of a separation bubble that bursts at $\alpha \approx 15°$. When stall takes place at $\alpha \approx 12°$, C_L is 38 % higher than its counterpart at $T_u = 0.6$ %. The enhancement of C_L as T_u increases is consistent with the results in the literature for the low to moderate Re_c data.[12, 43, 44] As T_u is further increased to 6.0 %, the peak in C_L is more pronounced and 51 % higher than that at $T_u = 0.6$ %. The observation suggests that, at least for $Re_c \leq 5.3 \times 10^3$, the stall can occur given adequately high turbulence intensity. It will be shown later that the increased T_u triggers the reattachment of separated flow, thus enhancing C_L. The effect of T_u on C_D is less significant. As shown in Figure IV-1 (b), the measured C_D values of different T_u rise monotonically and almost collapse for $\alpha < 10°$. Note that C_D at $T_u = 6.0$ % appears increasing more rapidly than at $T_u = 0.6$ % from $\alpha = 10$ to $12°$. So does that at $T_u = 2.6$ %. The observation is apparently linked to the occurrence of stall, which is always associated with an increase in drag. The lift-to-drag ratio C_L/C_D, proportional to the gliding ratio and climbing ability of the airfoil, is an important parameter to measure the aerodynamic efficiency of airfoil. Figure IV-1 (c) shows C_L/C_D against α for $Re_c = 5.3 \times 10^3$. Evidently, the increased T_u enlarges the maximum lift-to-drag ratio due to the increased C_L, from 3.2

at α = 10° for T_u = 0.6 % to 5.0 at α = 8° for T_u = 6.0 %, an increase by 56 %.

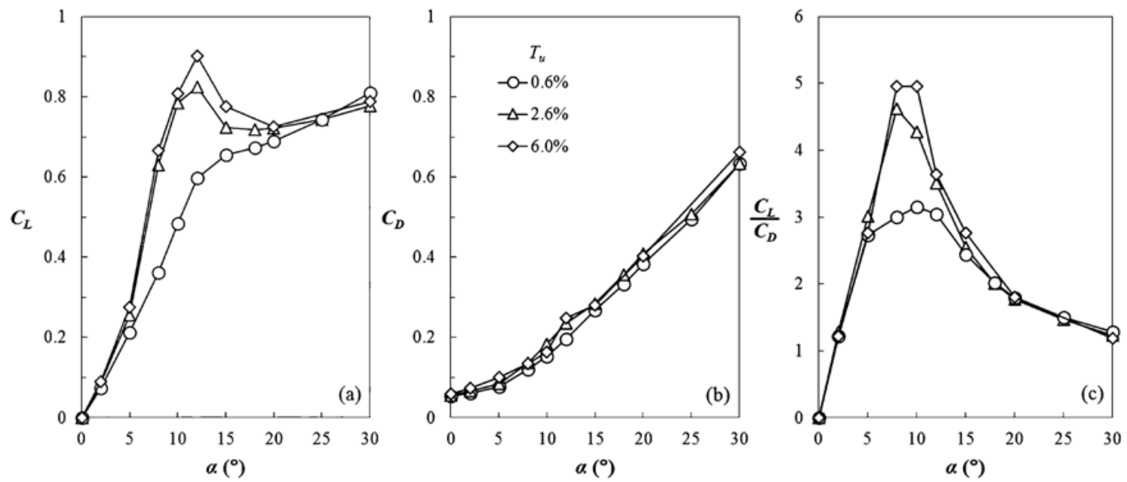

Figure IV-1. Dependence on α of C_L (a), C_D (b) and C_L/C_D (c) at different turbulence levels. $Re_c = 5.3 \times 10^3$.

In the low Re_c regime, the effect of T_u on C_D, C_L and C_L/C_D diminishes significantly, as illustrated at $Re_c = 2.0 \times 10^4$ in Figure IV-2 (a), though qualitatively similar to that in the ultra-low Re_c regime. At T_u = 0.6 %, C_L displays a peak, as observed by Alam *et al.*[8]. The peak is not sharp, corresponding to the burst of a long separation bubble.[40] The maximum C_L rises by 12 % with T_u increasing from 0.6 % to 6.0 %. This increase is much less than that (51 %) at $Re_c = 5.3 \times 10^3$, that is, the influence of T_u is greatly impaired from the ultra-low to the low Re_c regime, consistent with Huang and Lee[15]**.** At a higher T_u, the maximum C_L rises further, though very mildly. However, the peak turns to be sharp, showing a more abrupt drop in C_L at the occurrence of stall. This result suggests a change from the long separation bubble at $Re_c = 5.3 \times 10^3$ to a short one at higher T_u since a sharp fall in C_L corresponds to the leading edge stall characterized by the burst of a short separation bubble.[34, 40] With increased T_u, C_D varies little from α = 0 to 10° (Figure IV-2 b) but displays a discernible increase at α > 12° or after the stall. The observation is linked to the enhanced entrainment of free-stream fluid at higher T_u, which may cause a lower pressure in the recirculation region of the wake and give rise to the pressure drag on airfoil. There is little difference in C_L/C_D for different T_u (Figure IV-2 c) due to the cancellation effect of an increase in both C_L and C_D.

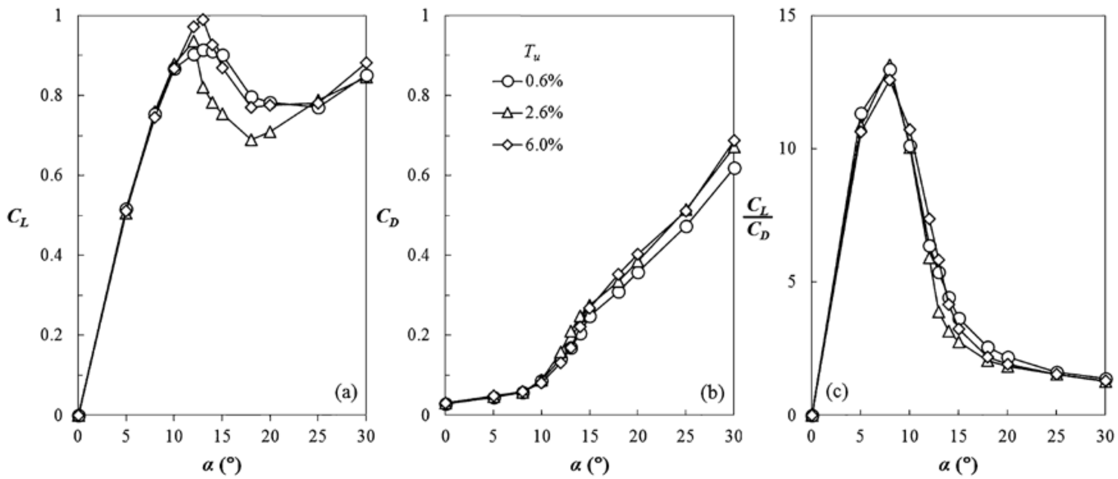

Figure IV-2. Dependence of C_L (a), C_D (b) and C_L/C_D (c) on α at different turbulence levels. $Re_c = 2.0 \times 10^4$.

The above results indicate that the T_u effect on the airfoil wake is more pronounced in the ultra-low Re_c regime because of a difference in the nature of flow separation.

B. Flow structure

The flow structure captured using qualitative LIF flow visualization and quantitative PIV is presented for $Re_c = 5.3 \times 10^3$ to understand the influence of T_u on the airfoil forces. Figure IV-3 compares the flow structure at T_u = 0.6 % and that at T_u = 6.0 %. The laminar boundary layer remains completely attached to the airfoil at α = 0° (Figure IV-3 a, i) but appears separated near the trailing edge at α = 2° (Figure IV-3 b, j) for both T_u levels. The observation suggests that the laminar boundary layer cannot withstand even a slight adverse pressure gradient that is present at α < 2° in the ultra-low Re_c regime. The separation point occurs at 0.60c and 0.63c from the leading edge for T_u = 0.6 % and 6.0 %, respectively, that is, the increased T_u acts to postpone flow separation, albeit slightly. The postponed separation is more evident at α = 5°, where flow separation takes place at 0.23c from the leading edge at T_u = 0.6 % (Figure IV-3 c) but at 0.45c at T_u = 6.0 % (Figure IV-3 k).

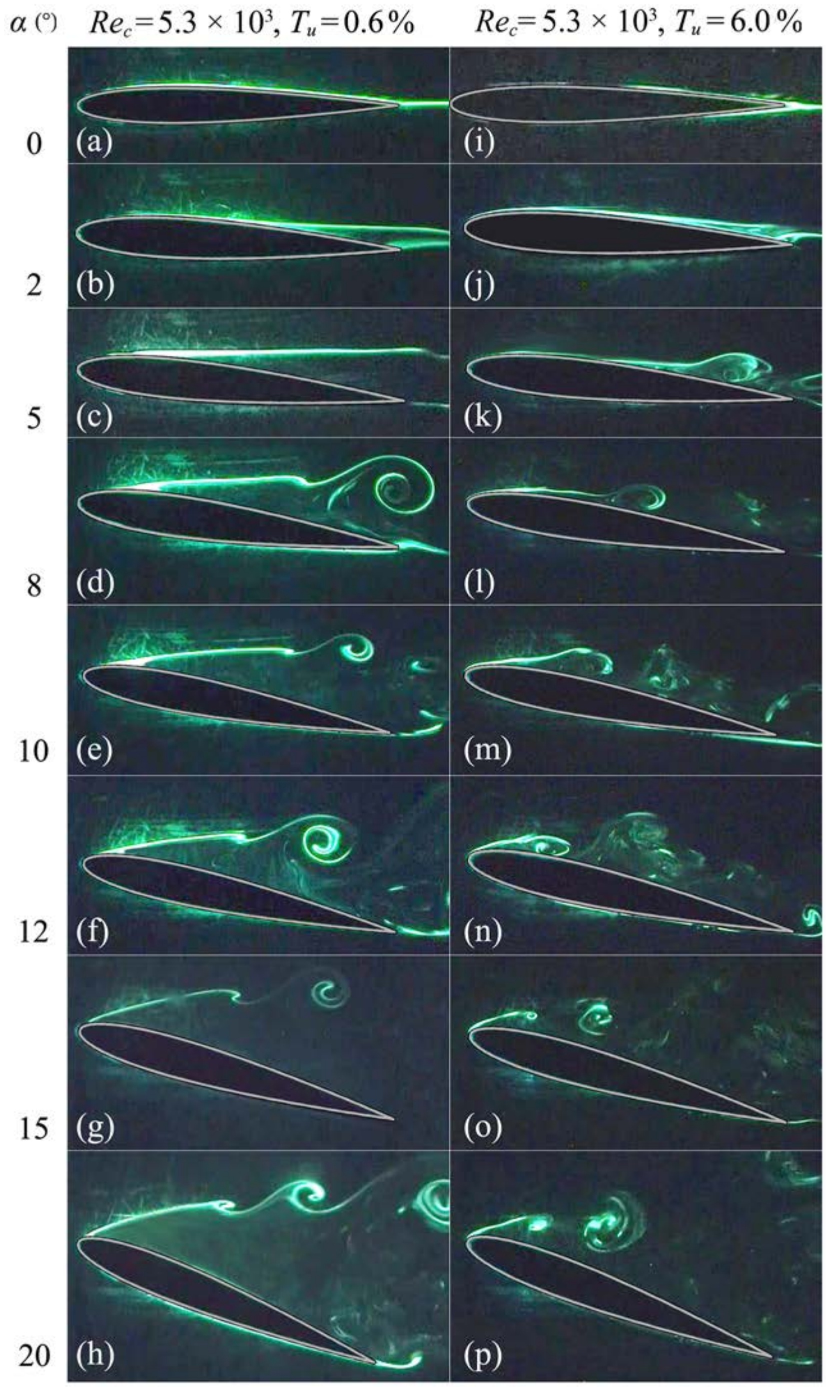

Figure IV-3. Typical photographs captured in LIF flow visualization for various α.

The separated shear layer develops more difference downstream. At $\alpha = 2°$, the upper shear layer is laminar for $T_u = 0.6$ % (Figure IV-3 b) without reattachment or mixing with the lower shear layer, at least within the extent of the image. But this layer appears mixed with the lower shear layer at the trailing edge for $T_u = 6.0$ % (Figure IV-3 j). This mixing suggests an enhanced entrainment ability of the wake due to the increased T_u. At $\alpha = 5°$, the upper shear layer at $T_u = 0.6$ % remains laminar for a long distance without reattachment (Figure IV-3 c). But at $T_u = 6.0$ % (Figure IV-3 k), the shear layer appears rolling up and experiencing transition shortly after separation and reattaches the airfoil surface at 0.8*c* from the leading edge. Obviously, the transition to turbulence has been advanced as a result of the increased T_u. The fact that the increased T_u acts to promote the shear layer transition is more evident at larger α. For example, at $\alpha = 15°$, the transition occurs at around 0.5*c* from the leading edge for $T_u = 0.6$ % (Figure IV-3 g) but at 0.2*c* for $T_u = 6.0$ % (Figure IV-3 o)**.** The advanced transition enhances greatly the entrainment and broadens the shear layer, resulting in reattachment. For both levels of T_u, the transition approaches gradually the separation point with α increased further, as reported.[42, 45]

Note that, at $T_u = 0.6$ %, the separated shear layer does not reattach the airfoil surface for any α presently examined (Figure IV-3 d-h), in agreement with Sunada *et al.*[46] observation from flow visualization over $\alpha = 6 \sim 16°$ at $Re_c = 4 \times 10^3$ for the same airfoil. At $T_u = 6.0$ %, in contrast, the separated shear layer reattaches at $\alpha \geqslant 5°$, producing a separation bubble. From $\alpha = 5$ to 12°, the reattachment point moves gradually towards the leading edge and the separation bubble appears shrinking in size (Figure IV-3 k-n). However, the upper shear layer fails to reattach the airfoil surface at $\alpha \geq 15°$ (Figure IV-3 o-p). As a result, the separation bubble disappears or bursts, forming a large recirculation zone.

The physical picture now emerges, which depends on the T_u level. For the ultra-low Re_c and low T_u, the separation point of the upper boundary layer moves from the trailing edge to the leading edge with increasing α; the separated shear layer remains laminar for a relatively long distance. As shown in Figure III-5, the flow structure change follows the pattern of A → B → C in the ultra-low Re_c regime. However, for the high T_u level, the upper separation point shifts towards the leading edge less rapidly, and the shear layer becomes turbulent shortly after separation. As such, the flow structure change follows the pattern of A → B → D → E → C, which is almost the same as in the low Re_c regime. The observation suggests some similarity in flow changes when increasing T_u and Re_c, respectively, which will be discussed along with disparity in the next section.

CHAPTER V. DISCUSSION

A. Similarity between the Re_c and T_u effects

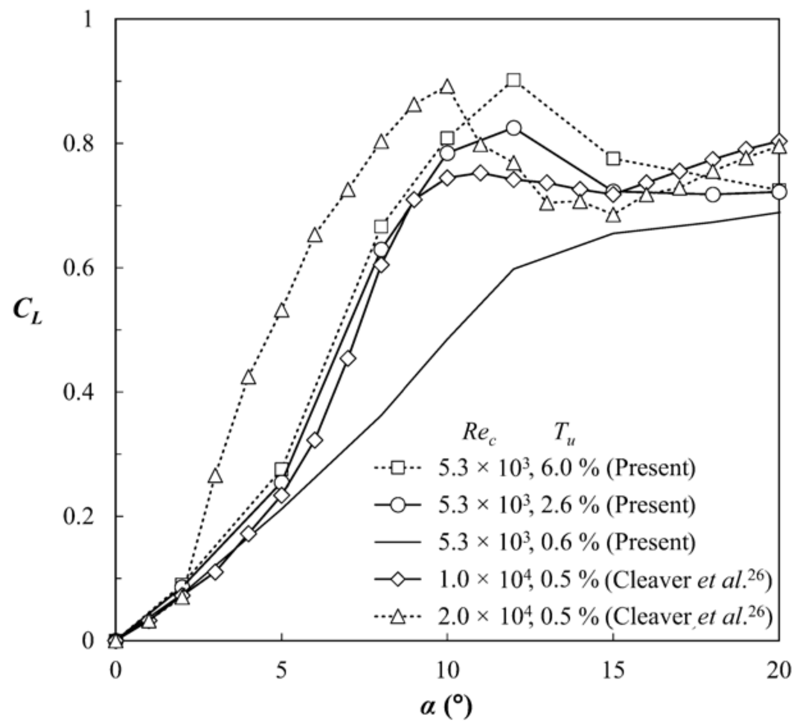

Figure V-1. Comparison between the Re_c and T_u effects on C_L.

As noted earlier, the effect of increasing T_u shows similarity to that of increasing Re_c. They both alter the C_L dependence on α, resulting in larger slope and $C_{L,\max}$ and hence a higher lift-to-drag ratio. Take the C_L–α relationship at $Re_c = 5.3 \times 10^3$ and $T_u = 0.6$ % (Figure V-1) as a reference, which is almost linear up to $\alpha = 12°$. The C_L–α relationship at $T_u = 2.6$ % appears quite similar to that at $Re_c = 1.0 \times 10^4$ for pre-stall α, with increasing and decreasing $dC_L/d\alpha$ from $\alpha = 3$ to 7° and 7 to 12°, respectively, which are connected to laminar and partially-laminar bubbles. In both cases, an earlier transition occurs in shear layer, causing flow reattachment and forming a separation bubble. The formation of the bubble has a positive effect on the aerodynamic performance of airfoil, increasing the maximum lift. When Re_c was further increased, the inflection point where $dC_L/d\alpha$ changes from increasing to decreasing is shifted, from $\alpha = 7°$ at $Re_c = 1.0 \times 10^4$ to $\alpha = 3°$ at $Re_c = 2.0 \times 10^4$. A similar observation is made, with the inflection point shifted to 5°, when T_u is increased to 6.0 %. In spite of a difference in pre-stalled C_L between $Re_c = 2.0 \times 10^4$ (T_u = 0.6 %) and T_u = 6.0 % ($Re_c = 5.3 \times 10^3$), $C_{L,\mathrm{max}}$ is enlarged to the same degree. It may be concluded that the effect of increasing Re_c bears close similarity to that increasing T_u.

B. Scaling parameter of the maximum lift

Quantitative equivalent relationship between T_u and Re_c could be established at least to some extent since increasing T_u produces almost the same effect as increasing Re_c, e.g. forming a separation bubble, enhancing transition in the shear layer, shifting the inflection point to lower α and enlarging $C_{L,\mathrm{max}}$. As far as $C_{L,\mathrm{max}}$ is concerned, the effect of a larger T_u can be treated as an addition of Re_c, that is, $C_{L,\mathrm{max}}$ at a lower Re_c and a non-zero T_u is equivalent to that at a higher Re_c and zero T_u.

This similarity was recognized in the moderate and high Re_c regimes as early as 1930s. Dryden and Kuethe[47] found that increasing T_u caused a decrease in the critical Reynolds number, $Re_{d,\mathrm{cr}}$ based on diameter d, of the sphere wake, at which the transition occurred in the boundary layer and drag coefficient dropped greatly, that is, increasing T_u hastened the transition in the boundary layer. They concluded that the flow about the sphere at a low Reynolds number in a wind tunnel was like that at a high Reynolds number in a non-turbulent stream. They conducted a similar test on streamlined airship models and predicted that the same concept could be applied for airfoil models. Inspired by this, Jacobs and Clay[48] referred to the low Reynolds number in a turbulent stream as the test Reynolds number Re (Re_d for the sphere and Re_c for the airfoil) and called the corresponding high Reynolds number, at which the similar flow state could occur in a non-turbulent stream, as the effective Reynolds number Re_{eff} ($Re_{d,\mathrm{eff}}$ for the sphere and $Re_{c,\mathrm{eff}}$ for the airfoil). He defined a turbulence factor TF, viz.

$$TF \equiv Re_{\mathrm{eff}} / Re, \tag{3}$$

and assumed it to be dependent only on T_u. TF serves to connect Re_c and $Re_{c,\mathrm{eff}}$ and removes the T_u effect. Once the TF-T_u correlation is established, the corresponding Re_{eff} could be determined from equation (3) for a given Re and T_u. Obviously, given $T_u = 0$, TF equals 1, resulting in $Re_{\mathrm{eff}} = Re$; TF grows with increasing T_u. Jacobs suggested two ways to determine TF, that is, comparing either the dependence of C_D on Re_d of the sphere wake or the dependence of $C_{L,\mathrm{max}}$ on Re_c of the airfoil wake obtained in a wind tunnel ($T_u \neq 0$) with that in flight tests conducted in free air ($T_u = 0$). The TF values determined from the two methods agreed with each other for the flight Re range, i.e. $Re > 1.0 \times 10^5$,[32, 49] though a possible difference may exist for $Re < 1.0 \times 10^5$.[48] The agreement lies in the fact that a higher T_u may incur the transition in the boundary layer, thus postponing flow separation, and this flow physics may affect equally the C_D-Re_d and $C_{L,\mathrm{max}}$-Re_c correlations. The sphere cylinder wake data is often used because the T_u effect may be easily quantified in terms of a change in $Re_{d,\mathrm{cr}}$, at which C_D drops abruptly. In contrast, there have been few attempts to use the airfoil wake data. Firstly, a Reynolds number has yet to be identified, which is representative, unique and sensitive to the T_u effect in the moderate to high Re_c regimes. Secondly, the $C_{L,\mathrm{max}}$ data base of various T_u is inadequate for the determination of TF. Based on Dryden and Kuethe's empirical correlation between $Re_{d,\mathrm{cr}}$ and T_u in the sphere wake[47], and the assumption that the effect of turbulence on the boundary layer transition is approximately the same for spheres and airfoils, Platt[49] applied TF = 3.85 ×

10^5 / $Re_{d,\mathrm{cr}}$, where 3.85×10^5 is the $Re_{d,\mathrm{cr}}$ in free air, for the airfoil wake at flight Re_c. Thus obtained correlations between $C_{L,\max}$ and $Re_{c,\mathrm{eff}}$ collapsed into a single curve,[32, 48, 49] albeit from a number of different wind tunnels with various T_u.

It would be interesting to know whether the data of $C_{L,\max}$ vs. $Re_{c,\mathrm{eff}}$ could collapse into one curve in the ultra-low and low Re_c regimes. We failed to see this collapse when $Re_{c,\mathrm{eff}}$ was calculated from $TF = 3.85 \times 10^5 / Re_{d,\mathrm{cr}}$. For example, at $Re_c = 2.0 \times 10^4$ and $T_u = 0.6\%$, reattachment occurs on the upper surface (Sec. IV). $Re_{d,\mathrm{cr}}$ would be 2.6×10^5 at $T_u = 0.6\%$ based on data from Dryden and Kuethe[47], and $TF = 3.85 \times 10^5 / Re_{d,\mathrm{cr}} = 3.85 \times 10^5 / 2.6 \times 10^5 = 1.5$. Then, the corresponding $Re_{c,\mathrm{eff}}$ should be $Re_c TF = 2.0 \times 10^4 \times 1.5 = 3.0 \times 10^4$, that is, a similar reattached flow should occur in a non-turbulent stream at an effective Reynolds number of 3.0×10^4. This is contradictory to the suggestion from Carmichael[50] that the minimum Reynolds number for the occurrence of reattachment is 5.0×10^4 in a non-turbulent stream for most common airfoils. A similar contradiction is found at $Re_c = 5.3 \times 10^3$. The T_u effect on the airfoil wake is grossly underestimated in the ultra-low and low Re_c regimes if the classical TF (= $3.85 \times 10^5 / Re_{d,\mathrm{cr}}$) is simply applied. It may be concluded that the classical TF-T_u correlation, based on the sphere wake data, cannot be extended to the low and ultra-low Re_c regimes. Physically, $Re_{d,\mathrm{cr}}$ occurs only at the moderate to high Re_c and cannot be connected to the T_u effect at very low Re_c. This verifies the assertion from Jacobs and Sherman[32] that the classical TF was suitable only over the flight range of the Reynolds number. They did not examine the range of Reynolds Number below the usual flight range, though recognizing its fundamental importance, due to a lack of practical applications at that time, along with the poor measurement accuracy in low Reynolds number airfoil experiments.

One may naturally beg the question how to determine *TF* in the ultra-low and low Re_c regimes. To this end, we propose to compare $Re_{c,\mathrm{cr}}$, identified from the dependence of $C_{L,\max}$ on Re_c, obtained in a wind tunnel ($T_u \neq 0$) with its counterpart in free air ($T_u = 0$). The choice of $Re_{c,\mathrm{cr}}$ is due to a number of considerations. Firstly, unlike $Re_{d,\mathrm{cr}}$, $Re_{c,\mathrm{cr}}$ lies in the Re_c range of concern. Secondly, $Re_{c,\mathrm{cr}}$ is the critical Reynolds number between the ultra-low and low Re_c regimes and is easy to identify. As shown in the dependence of $C_{L,\max}$ on Re_c (Figure III-4), there is an abrupt increase in $C_{L,\max}$ at $Re_{c,\mathrm{cr}}$ with rising Re_c. Also, there is one pronounced peak (stall) for $Re_c > Re_{c,\mathrm{cr}}$ but none for $Re_c < Re_{c,\mathrm{cr}}$ in the C_L dependence on α (Figure III-1). Thirdly, $Re_{c,\mathrm{cr}}$ in free air ($T_u = 0$) could be estimated from previously reported data, which is crucial to determine quantitatively the relationship of $TF = TF(Re_{c,\mathrm{cr}})$. Based on his comprehensive survey of test data from different laboratories, Carmichael[50] stated that, for most common airfoils, under natural laminar separation conditions, the distance from separation to reattachment could be expressed as $Re_\mathrm{R} - Re_\mathrm{S} = 5.0 \times 10^4$, where Re_R and Re_S were chord Reynolds numbers based on distances from the leading edge to the separation and reattachment points, respectively. We may then infer $Re_{c,\mathrm{cr}} = 5.0 \times 10^4$ in free air in view of the definition of $Re_{c,\mathrm{cr}}$. Finally, a number of $Re_{c,\mathrm{cr}}$ is available for various T_u from present measurements and previous reports, allowing the variation in $Re_{c,\mathrm{cr}}$ to be correlated with T_u. Huang and Lin[51] classified the characteristic flow modes of NACA 0012 for $Re_c = 3.0 \times 10^3 \sim 1.2 \times 10^5$ in a wind tunnel with $T_u = 0.2$ %, suggesting a $Re_{c,\mathrm{cr}}$ between 2.0×10^4 and 4.0×10^4. The present LIF and PIV data clearly indicates the formation of a LSB for $Re_c = 2.0 \times 10^4$ and the absence of the bubble for $Re_c = 5.3 \times 10^3$ at $T_u = 0.6$ %, suggesting a $Re_{c,\mathrm{cr}}$ between 2.0×10^4 and 5.3×10^3. Similarly, the $Re_{c,\mathrm{cr}}$ is estimated to be less than 5.3×10^3 at $T_u = 2.6$ % and 6.0 % based on the observed formation of LSBs.

Figure V-2 presents the correlation between $Re_{c,\mathrm{cr}}$ and T_u, where the upper and lower bars indicate the range of uncertainty. Evidently, $Re_{c,\mathrm{cr}}$ drops rapidly as T_u increases from 0% to 0.6% and then slowly for higher T_u. This is because at a higher T_u a smaller Re_c is required to promote the transition in the shear layer. Noting that $TF \equiv Re_{c,\mathrm{eff}} / Re_c$ and $Re_{c,\mathrm{eff}} = Re_c = 5.0 \times 10^4$ at $T_u = 0$ based on Figure V-2, we may find

$$TF = 5.0 \times 10^4 / Re_{c,\mathrm{cr}}. \qquad (4)$$

In arriving at equation (4), we have invoked the assumption that *TF* is dependent only on T_u. In view of the relation between $Re_{c,\mathrm{cr}}$ and T_u (Figure V-2), we may correlate *TF* and T_u from equation (4), as shown in Figure V-3. This relation is good for the ultra-low to low Re_c regimes of the airfoil wake. The classical data of *TF*, obtained from the sphere wake, is also given in the figure, which is valid only for the moderate to high Re_c regimes.[48] Despite of different methods involved in determining *TF*, their physical implication should be the same for the two *TF* curves. The *TF* is significantly larger in the ultra-low to low Re_c regimes than in the moderate to high Re_c regimes, highlighting the enhanced T_u effect in the former regimes. From equation (3), we then have

$$Re_{c,\mathrm{eff}} = Re_c \times (3.85 \times 10^5 / Re_{d,\mathrm{cr}}), \qquad Re_c > 3.0 \times 10^5 \qquad (5\text{-}1)$$

$$Re_{c,\mathrm{eff}} = Re_c \times (5.0 \times 10^4 / Re_{c,\mathrm{cr}}), \qquad Re_c < 3.0 \times 10^5 \qquad (5\text{-}2)$$

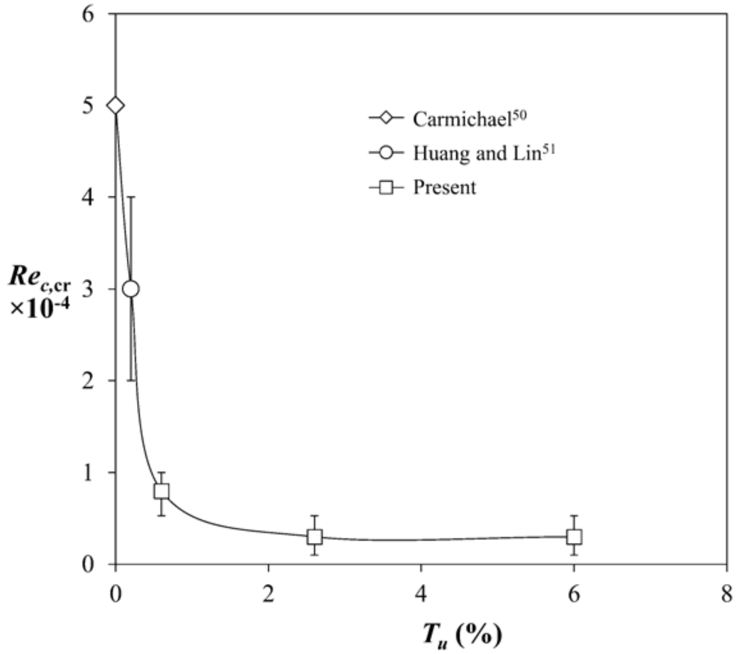

Figure V-2. Dependence on T_u of the critical Reynolds number $Re_{c,\mathrm{cr}}$, which divides the ultra-low and low Re_c regimes.

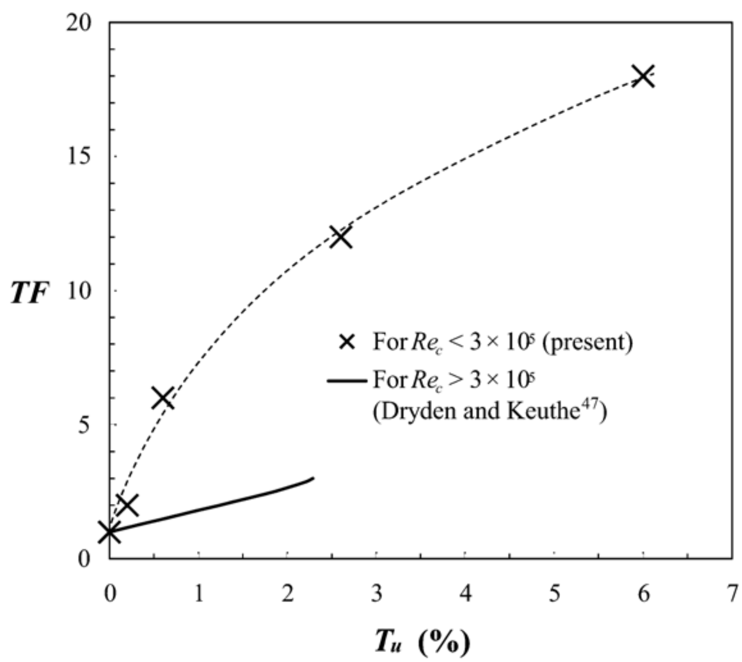

Figure V-3. Dependence of turbulence factor *TF* on T_u for NACA 0012 in the ultra-low and low Re_c regimes.

Figure V-4 (a) presents the variation in $C_{L,\max}$ with $Re_{c,\mathrm{eff}}$, collected from the literature as well as ours. The data from Jacobs and Sherman[32] covers the moderate and high Re_c

regimes. Most of the data collapse essentially into a single curve, in distinct contrast to the considerable scattering in the $C_{L,\max}$-Re_c relation (Figure V-4 b). A certain degree of departure is expected; after all, the data was measured in different facilities using different techniques. The observation demonstrates unequivocally that $C_{L,\max}$ is scaled with $Re_{c,\text{eff}}$. Note that the $C_{L,\max}$-$Re_{c,\text{eff}}$ relationship agrees qualitatively with that between $C_{L,\max}$ and Re_c (Figure III-4), thus providing a validation for the presently estimated *TF*, which is crucial for establishing the equivalence between Re_c and T_u in the airfoil wake of the ultra-low to low Re_c regimes. The critical $Re_{c,\text{eff}}$ that divides the ultra-low and low Re_c regimes in the ideal non-turbulent free-stream ($T_u = 0$) is 5.0×10^4, which is 5 times $Re_{c,\text{cr}}$ (Figure III-4) obtained from actual experimental conditions ($0 < T_u \leqslant 1$ %). Similarly, the other two critical Reynolds numbers that separate the low, moderate and high Reynolds number regimes are also shifted to larger values in the ideal non-turbulent free-stream: from 3×10^5 and 5×10^6 to 8×10^5 and 6×10^6 respectively. In view of the physical meaning of $Re_{c,\text{eff}}$, Figure V-4 presents the dependence of $C_{L,\max}$ on the Reynolds number in the ideal non-turbulent free-stream.

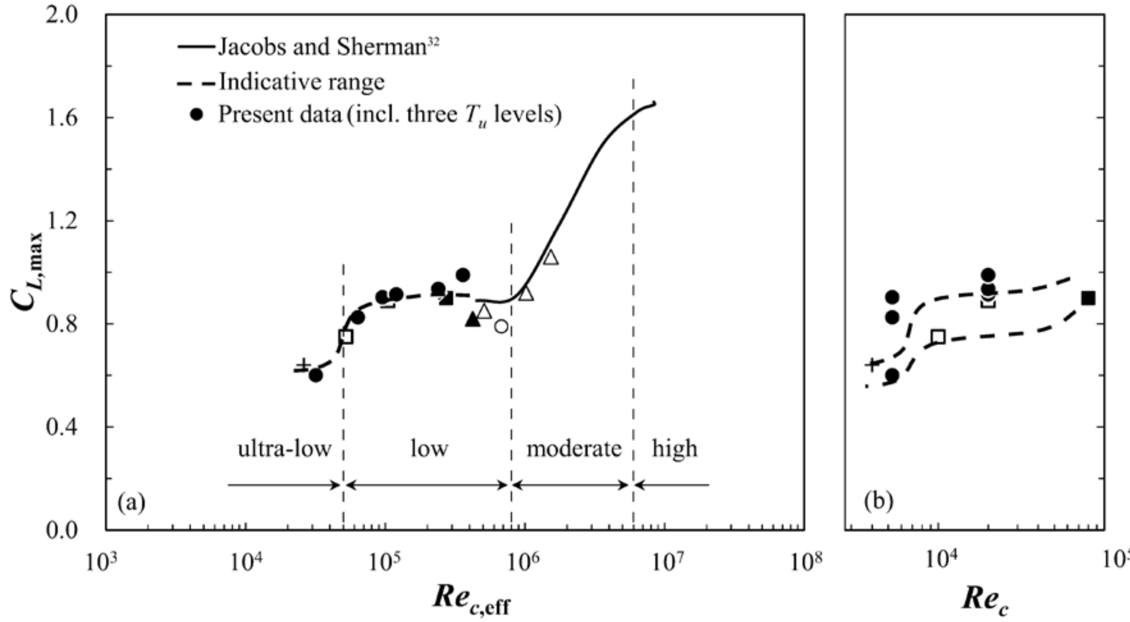

Figure V-4. Dependence of the maximum lift coefficient $C_{L,\max}$ on (a) effective Reynolds number $Re_{c,\text{eff}}$, (b) test Reynolds number Re_c: +Sunada *et al.*[25]; ■ Chen and Choa[35]; □ Cleaver *et al.*[26]; ○ Grager *et al.*[36]; ◆ Lee and Gerontakos[37]; ▲ Wong and Kontis[38]; △ Sant and Ayuso[39].

C. Difference between the Re_c and T_u effects

The influences of T_u and Re_c on flow separation are opposite to each other. An increase in T_u postpones flow separation; yet an increase in Re_c promotes early separation, followed by reattachment. To our best knowledge, this has not been reported previously. Figure V-5 presents instantaneous snapshots of the flow structure captured from LIF flow visualization and the iso-contours of PIV-measured $\overline{U}^*$, where the effect of increasing Re_c on the separation point is compared with that of increasing T_u ($\alpha = 5°$). As indicated in the snapshots, the separation point is postponed from 0.23*c*, from the leading edge, at T_u = 0.6 % (Figure V-5 c) to 0.45*c* at T_u = 6.0 % (Figure V-5 a). On the other hand, given T_u = 0.6 %, this point moves from 0.23*c* at $Re_c = 5.3 \times 10^3$ to 0.18*c* at $Re_c = 2.0 \times 10^4$ (Figure V-5 e). The $\overline{U}^*$-contours re-confirm this observation. Note that, for given Re_c and T_u (e.g. Figure V-5 a, b), the separation points identified from the instantaneous PIV images and the $\overline{U}^*$ -contours may not occur at exactly the same position because of the unsteady nature of the separation point.

The normalized separation point position x^*_{sep} from the leading edge, extracted from the time-averaged PIV data, depends on *α,* as summarized inFigure V-6. The separation point moves to the leading edge with increasing *α,* irrespective of the combination of T_u and Re_c. The separation point at $Re_c = 5.3 \times 10^3$ moves closer to the leading edge from $T_u = 0.6$ % to 6.0 %. However, given $T_u = 0.6$ %, this point moves in the opposite direction from $Re_c = 5.3 \times 10^3$ to 2.0×10^4, indicating the opposite effect of increasing T_u and increasing Re_c on the separation point at $\alpha = 5 \sim 20°$.

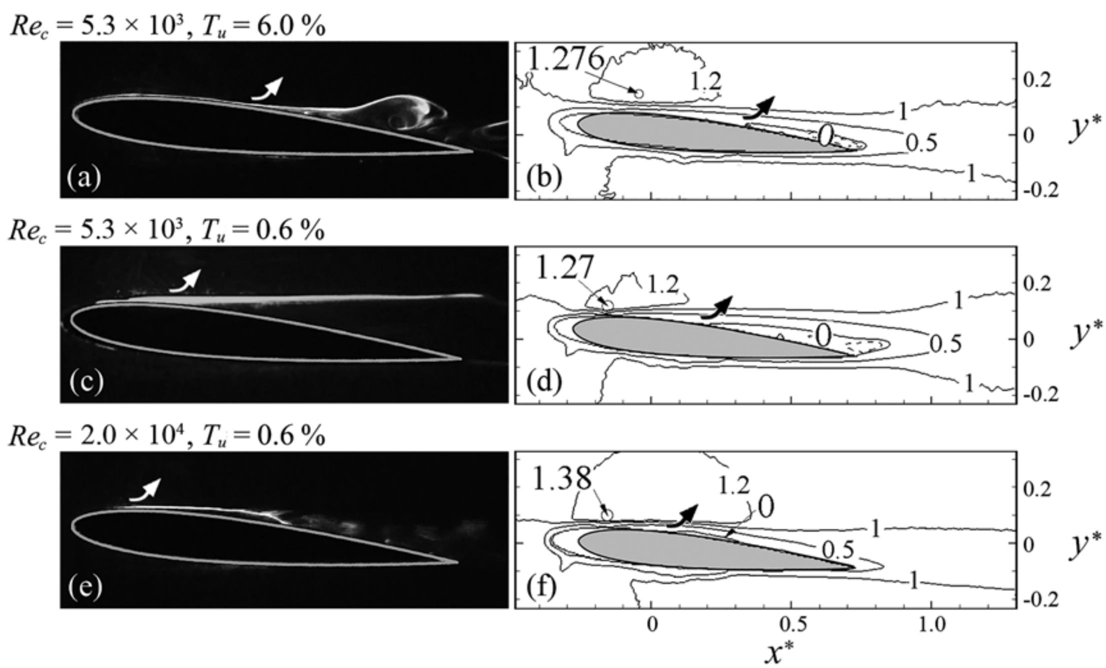

Figure V-5. Effect of Re_c or T_u on the flow separation point at $\alpha = 5°$. Left column: photographs of instantaneous flow structure captured from LIF flow visualization; right column: iso-contours of PIV-measured time-averaged streamwise velocity $\overline{U}^*$. Symbol indicates the occurrence of flow separation.

This opposite effect was also observed on a SD7003 airfoil in low Re_c range ($Re_c = 2.1 \times 10^4 \sim 4.6 \times 10^4$) by Olson *et al.*[52], though without any explanation. Aubertine[53] investigated the effect of Reynolds number on the adverse pressure gradient boundary layer developed along a 4° ramp and noted an increasing adverse pressure gradient with increasing Reynolds number. This may provide a clue on the present observation, that is, increased Re_c may incur an increase in the adverse pressure gradient and hence early separation. On the other hand, as T_u grows from 0.6 % (Figure V-5 d) to 6.0 % (Figure V-5 b), the occurrence of $\overline{U}^*_{max}$, though changing little in magnitude, is shifted appreciably downstream. So is the separation position. The increased T_u can enhance the mixing of the boundary layer with high momentum free-stream fluid, resulting in the postponed flow separation.

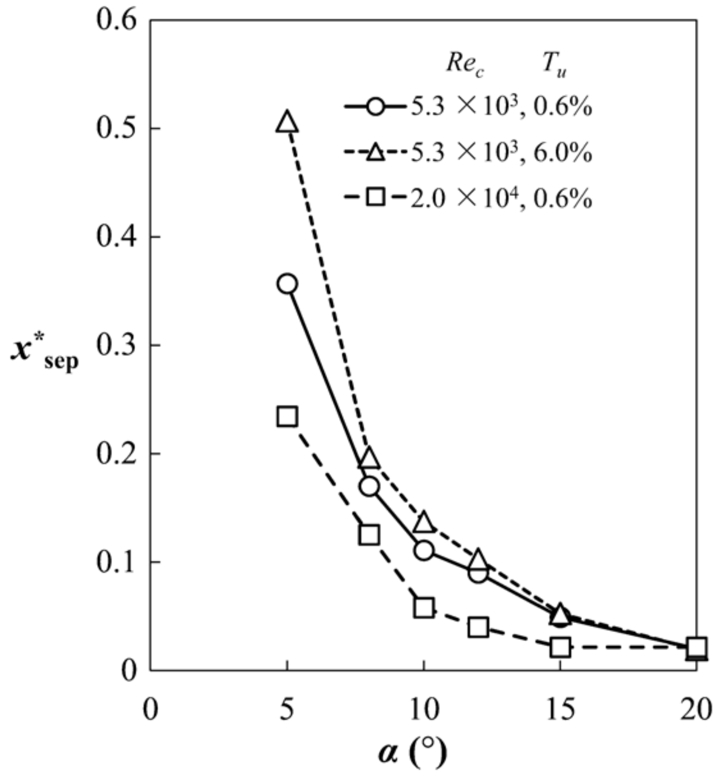

Figure V-6. Dependence of the flow separation point x^*_{sep} on α.

Both flow structure and stall depend not only on Re_c and T_u but also on the airfoil shape including thickness, camber, etc. The shape effect on the flow structure can be different for different Re_c regimes. The shape effect can be significant, influencing the transition, separation, reattachment, etc., in the moderate and high Re_c regimes where the boundary layer is attached/reattached over a longer length of the airfoil at relatively large α than in the other two regimes (Fig. 8). In the other two Re_c regimes, in particular at ultra-low Re_c, the boundary layer separates at smaller α, with transition occurring late in the free shear layer (Fig. 8). Once the boundary layer is separated, the afterbody shape has little influence on flow. The deterioration of the aerodynamic performance in the ultra-low Re_c regime is primarily due to the absence of the separation bubble. A simple change in the airfoil geometry, such as increasing camber or moving the position of the maximum camber backwards, may not effectively promote the transition or formation of bubble, and therefore may not affect significantly the airfoil performance.

D. Criteria for bursting of the separation bubble

Gaster developed a general criteria in 1967 for predicting conditions that lead to a burst of short separation bubble.[56] He studied a laminar separation bubble on flat plate and proposed a criterion to predict when the short bubble will burst into long bubble. The method is based on two parameters, the momentum-thickness Reynolds number ($Re_{\theta,\mathrm{sep}}$) and a dimensionless velocity gradient (sometimes called a dimensionless pressure gradient and hence denoted by ΔP_{avg}),

$$\Delta P_{\mathrm{avg}} = \frac{\theta_{\mathrm{sep}}^2}{\nu}\frac{\Delta U}{\Delta x}. \quad (6)$$

The velocity gradient can be obtained from an inviscid flow analysis without separation. Gaster obtained this gradient by measuring the pressure distribution when the separation has been inhibited by tripping the boundary layer, which is an approximation to the inviscid pressure distribution if the boundary layer thickness is negligible.

As the present investigation involves the onset and burst of the laminar separation bubble, it is of interest to examine whether the general separation criteria still hold in the ultra-low to low Reynolds number regimes. The momentum thickness of the boundary layer at separation and the length of the separation bubble can be estimated from PIV-measured time-averaged velocity. Following discussion is made firstly on the characteristics of the time-averaged LSB and then on the correlation criteria.

Figure V-7 shows typical PIV-measured time-averaged velocity vectors and the $\overline{U}$ -contours of the separation bubble at $\alpha = 5°$ ($Re_c = 2.0 \times 10^4$), which clearly outline the shape of LSB. The scale in the *y* direction is enlarged to improve the visibility of the bubble. As discussed earlier, the boundary layer changes from laminar to turbulent between the separation and reattachment points. The normalized velocity (U^*_e) at the outer edge of the boundary layer, minimum streamwise velocity (U^*_{min}, associated with reversed flow) and momentum thickness (θ) on the suction side of the airfoil were estimated and plotted against *x*/*c* in Figure V-8. Inviscid velocity distribution is included in Fig. 19 for the purpose of comparison, obtained using Xfoil, a commonly used and well validated code in airfoil analysis by Drela.[57] The major characteristics of LSB can be easily extracted as follows. The maximum U^*_e near the leading edge represents the suction peak. Flow passing beyond the suction peak encounters an adverse pressure gradient, but remains attached until the separation point. U^*_e decreases and θ increases gradually along *x*/*c* in this area. Starting from the separation point, U^*_e and θ maintain constant up to the transition point. U^*_{min} drops from zero to a negative value at first, and then tends to be constant in this *x/c* range. After the transition occurs in the separated boundary layer, turbulent mixing reduces $U^*_{e,}$ resulting in reattachment. In the turbulent region, θ grows rapidly, while U^*_{min} firstly drops to a minimum value and then recovers to zero, which is in agreement with Gaster's measurements.[56] After reattachment, the turbulent boundary layer forms, with mildly decreasing U^*_e, increasing θ and zero U^*_{min}.

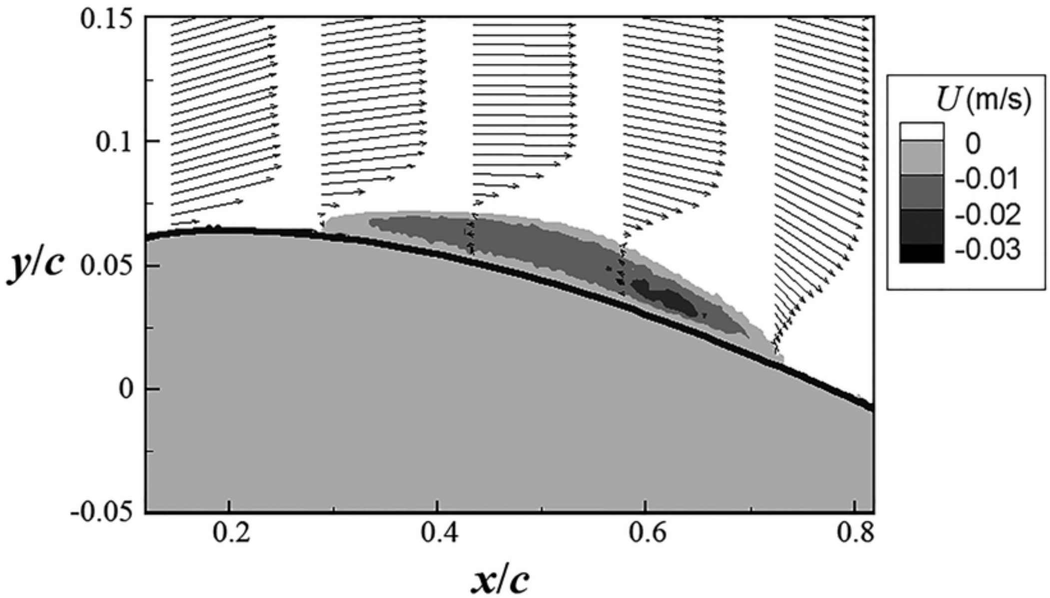

Figure V-7. Velocity vectors and the $\overline{U}$ -contours of the separation bubble at α = 5°. $Re_c = 2.0 \times 10^4$. The scales of *x* and *y* are different.

The normalized length of LSB (L^*_{LSB}) and momentum thickness at separation (θ_{sep}) are plotted against α for cases where LSB was visible, as shown in Figure V-9. As α climbs, L^*_{LSB} retreats to a minimum value before the bubble bursts for both flow conditions, i.e. $Re_c = 5.3 \times 10^3$ at T_u = 6.0% and $Re_c = 2.0 \times 10^4$ at T_u = 0.6%. Following Gaster's definition,[56] we refer to the condition at which L^*_{LSB} reaches the minimum as the critical point for the LSB bursting. Under both flow conditions, θ_{sep} drops with increasing α, resulting from the forward-shifted separation point.

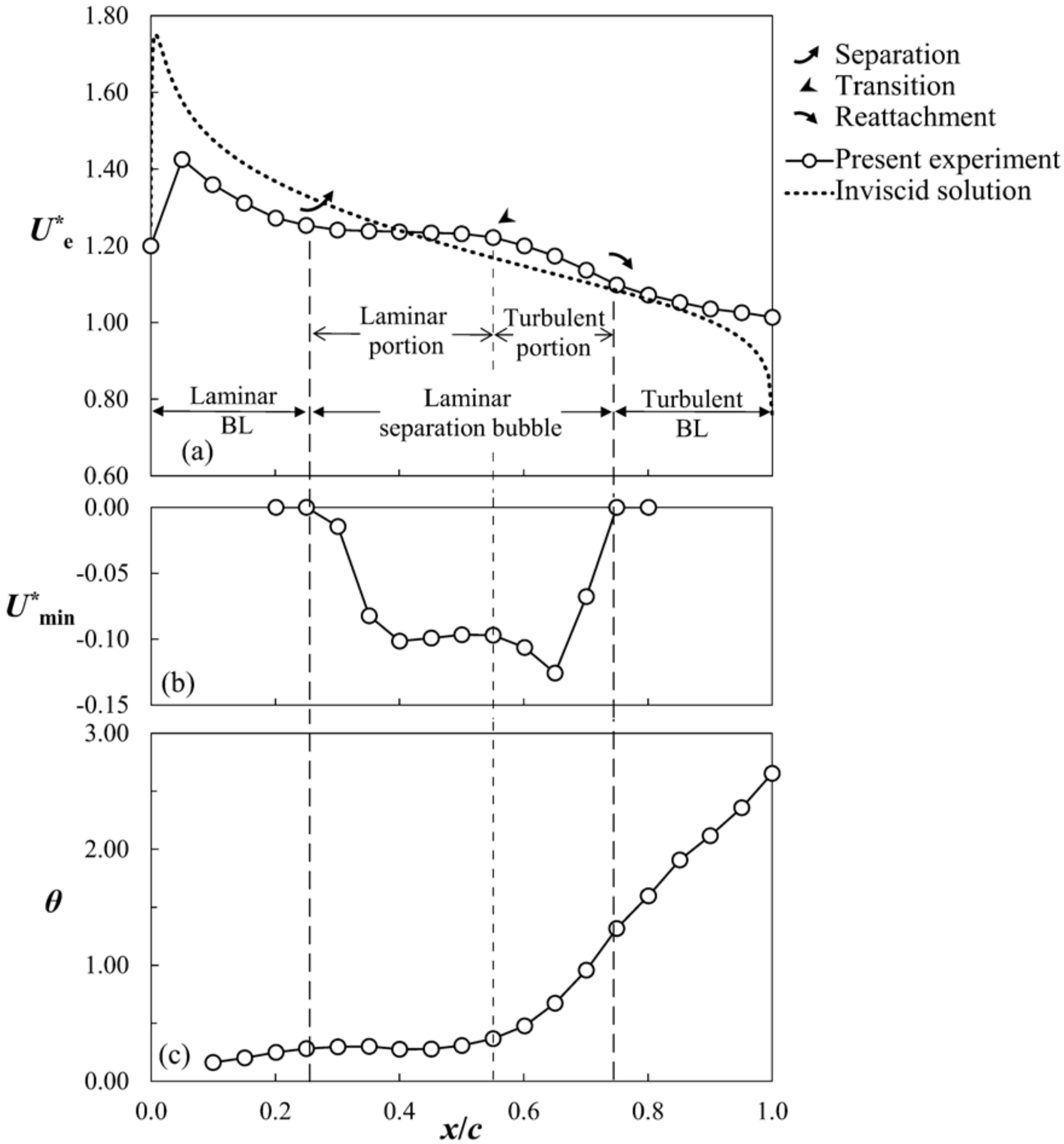

Figure V-8. (a) Normalized boundary layer edge velocity U^*_{e}, (b) normalized minimum velocity U^*_{min}, and (c) momentum thickness θ of the boundary layer at $\alpha = 5°$. $Re_c = 2.0 \times 10^4$.

Figure V-10 compares the presently obtained ΔP_{avg} with the criterion curve proposed by Gaster. As shown by the solid line, his criterion curve does not include data for $Re_{\theta,\mathrm{sep}} < 130$. A simple extrapolation of this curve to lower $Re_{\theta,\mathrm{sep}}$, marked by the dashed curve, results in considerably lower ΔP_{avg} than the present result, denoted by the dotted line. This indicates a failure to apply Gaster's bursting criterion to the low and ultra-low Re_c regimes. One possible reason for the large discrepancy may come from the estimate of ΔP_{avg}. Gaster obtained this value by tripping the laminar boundary layer to a turbulent one, which remained attached, rather than by the direct inviscid analysis of the pressure distribution. The inviscid analysis is based on the ideal airfoil section and dismisses the displacement effect of the actual boundary layer, but the experimental tripped-boundary-layer method is affected by the thickness of actual boundary layer. Though the deviation produced by the two methods is negligible for the moderate to high Re_c regimes due to a thin boundary layer, it is not so for the ultra-low to low Re_c regimes, because the displacement effect of the boundary layer cannot be neglected, where the boundary layer thickness is rather thick.

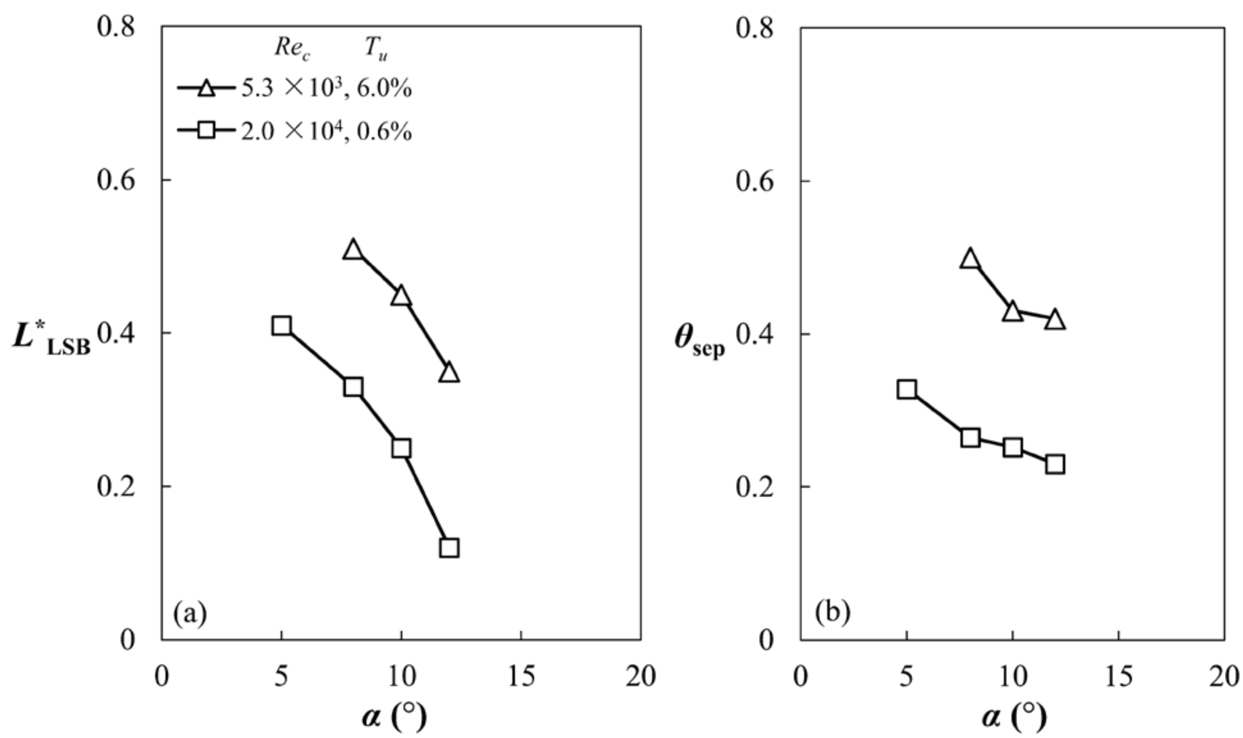

Figure V-9. Dependence of the laminar separation bubble (LSB) on α: (a) normalized bubble length L^*_{LSB} and (b) momentum thickness θ_{sep} of the boundary layer at separation.

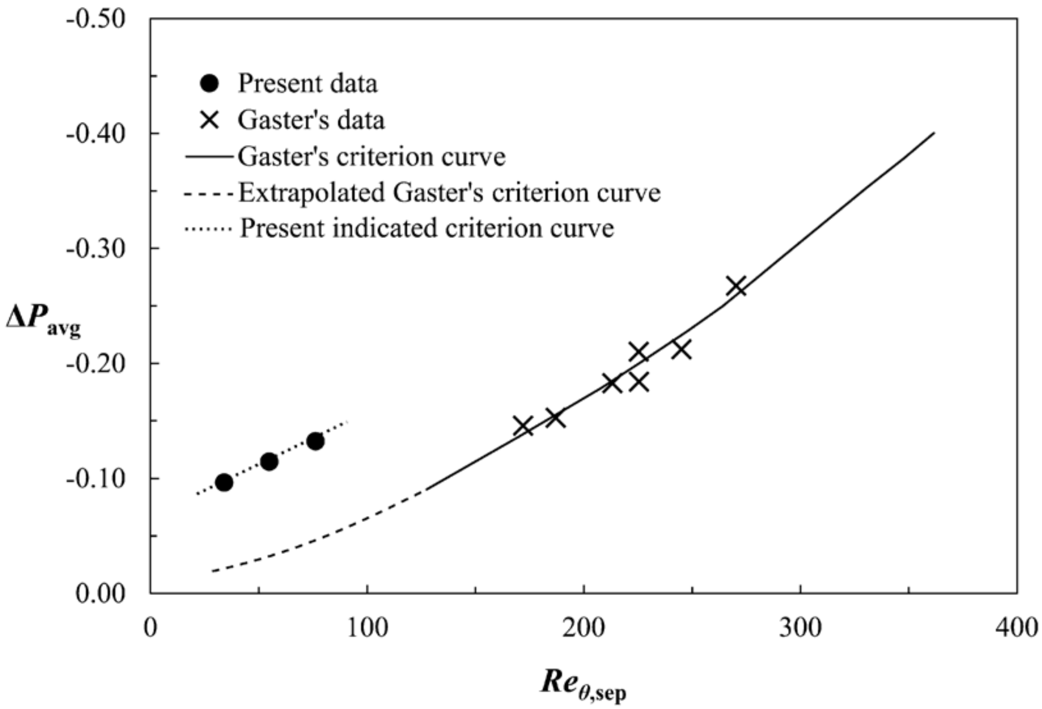

Figure V-10. Relation between $Re_{\theta,\mathrm{sep}}$ and ΔP_{avg} at bursting.

CHAPTER VI. CONCLUSIONS

Investigation has been experimentally carried out on the aerodynamics in the wake of an NACA 0012 airfoil for $Re_c = 5.3 \times 10^3$ and 2.0×10^4. Following conclusions can be drawn:

(1) Four Re_c regimes have been proposed for the first time, i.e. the ultra-low ($< 1.0 \times 10^4$), low ($1.0 \times 10^4 \sim 3.0 \times 10^5$), moderate ($3.0 \times 10^5 \sim 5.0 \times 10^6$) and high ($> 5.0 \times 10^6$) regimes, each exhibiting distinct characteristics in terms of its $C_{L,\max}$-Re_c relationship and flow structure dependence on α. The separated laminar shear layer does not reattach in the ultra-low Re_c regime but does, forming a separation bubble, in the low Re_c regime. The transition to turbulence occurs after reattachment at small α and before reattachment at large α. The moderate Re_c regime is also associated with a separation bubble, though the transition takes place before reattachment, closer to the separation point. On the other hand, the transition occurs in the boundary layer, prior to flow separation, in the high Re_c regime.

(2) In the four Re_c regimes, eight distinct flow structures are observed on the suction side of the airfoil, namely, flow structures A (fully attached laminar boundary layer), B (partially attached laminar boundary layer), C (fully separated laminar shear layer), D (laminar bubble), E (partially laminar bubble), F (fully attached turbulent boundary layer), G (trailing-edge-separated turbulent boundary layer) and H (fully separated turbulent shear layer). With increasing α, the flow structure changes and the sequence is A→B→C in the ultra-low Re_c regime, B→D→ E→stall type I→C in the low Re_c regime, E→stall type II→C in the moderate Re_c, and F→G →stall type III→H in the high Re_c regime.

(3) All the C_L data collapses for $\alpha < 2 \sim 5°$, with the exact α range depending on Re_c and increases for a smaller Re_c, in the ultra-low and low Re_c regimes. The corresponding slope

$dC_L/d\alpha$ is 0.038, different from the well-known slope of 0.11 for an airfoil at small α in the high Re_c regime. The laminar and turbulent boundary layers attaching on most of the airfoil lead to the former and latter slopes, respectively. For $\alpha > 2 \sim 5°$, C_L increases almost linearly to $C_{L,\max}$ in the ultra-low Re_c regime and nonlinearly in the low Re_c regime where $dC_L/d\alpha$ may increase and decrease. While the linear variation is associated with the rollup of laminar shear layer over the airfoil surface without reattachment, the increasing and decreasing $dC_L/d\alpha$ are connected to reattaching shear layer with transition after and before reattachment, respectively.

(4) In the ultra-low Re_c regime, the influence of T_u is significant. Stall does not occur at T_u = 0.6 % but does at T_u = 2.6 % and 6.0 %. With increased T_u, flow separation is postponed and the transition occurs in the separated shear layer, which may induce flow reattachment and improve significantly the aerodynamic performance of airfoil. For example, at $Re_c = 5.3 \times 10^3$, the maximum C_L and C_L/C_D can be increased by 52 % and 45 %, respectively, from T_u = 0.6 % to 6.0 %. This increase is comparable with that due to increasing Re_c in the ultra-low Re_c regime. In the low Re_c regime, the T_u effect wanes. For example, stall occurs at $Re_c = 2.0 \times 10^4$, regardless of the level of T_u. The maximum C_L is increased by only 10 % and the maximum C_L/C_D does not even change from T_u = 0.6 % to 6.0 %.

(5) The influence of T_u on the airfoil wake exhibits similarity to that of Re_c. Given a higher value, both T_u and Re_c may increase $C_{L,\max}$ or maximum C_L/C_D and may cause early transition in the shear layer and hence reattachment, forming a separation bubble. As such, the concept of the effective Reynolds number, which treats T_u as additional Re_c in the moderate and high Re_c regimes, is extended and validated in the low and ultra-low Re_c

regimes. Nevertheless, there is a difference between the two effects. The increased T_u postpones flow separation due to enhanced mixing; but the increased Re_c causes a more pronounced adverse pressure gradient, which changes little with T_u, in the boundary layer and thus promotes flow separation.

(6) It has been found that $C_{L,\max}$ at different T_u displays considerable scattering if plotted against Re_c but collapses into one single curve if Re_c is replaced by $Re_{c,\mathrm{eff}}$, that is, $C_{L,\max}$ is scaled with $Re_{c,\mathrm{eff}}$ (= $TF\ Re_c$). Whilst $Re_{c,\mathrm{eff}}$ was estimated based on the critical Reynolds number, at which the transition occurs in the boundary layer of the sphere wake, for the moderate and high Re_c regimes, it is presently determined based on the critical Reynolds number $Re_{c,\mathrm{cr}}$ that divides the ultra-low and low Re_c regimes and is given by $Re_{c,\mathrm{eff}} = 5.0 \times 10^4 / Re_{c,\mathrm{cr}}$. The $Re_{c,\mathrm{cr}}$ depends strongly on T_u, decreasing rapidly from 5.0×10^4 at T_u = 0 to 7.8×10^3 at T_u = 0.6% and then displays a slow drop to 5.3×10^3 at T_u = 6.0%.

(7) A simple extrapolation of the classical two-parameter bursting criterion for short laminar separation bubble does not apply to present cases in ultra-low and low Re_c regimes. A new criteria line is suggested to be validated for $Re_{\theta,\mathrm{sep}}$ less than 100, where $Re_{\theta,\mathrm{sep}}$ is the momentum thickness based Reynolds number at the separation of boundary layer.

REFERENCES

[1] M. Brendel and T. J. Mueller, "Boundary-layer measurements on an airfoil at a low Reynolds-number in an oscillating freestream," AIAA J **26** (3), 257-263 (1988).

[2] F.-b. Hsiao, C.-f. Liu and Z. Tang, "Aerodynamic performance and flow structure studies of a low Reynolds number airfoil," AIAA J **27** (2), 129-137 (1989).

[3] J. C. M. Lin and L. L. Pauley, "Low-Reynolds-number separation on an airfoil," AIAA J **34** (8), 1570-1577 (1996).

[4] T. J. Mueller, "Aerodynamic measurements at low Reynolds numbers for fixed wing micro-air vehicles," DTIC No. ADP010760 (1999).

[5] D. Pines, "Nano air vehicle (nav) program," in *Proposer Information Pamphlet for Defense Advanced Research Projects Agency*, edited by D. A. R. P. Agency (BAA 06-06, 2005).

[6] Z. J. Wang, "Dissecting insect flight," Annu Rev Fluid Mech **37** (1), 183-210 (2005).

[7] T. J. Mueller and J. D. DeLaurier, "Aerodynamics of small vehicles," Annu Rev Fluid Mech **35** (1), 89-111 (2003).

[8] M. M. Alam, Y. Zhou, H. X. Yang, H. Guo and J. Mi, "The ultra-low Reynolds number airfoil wake," Exp Fluids **48** (1), 81-103 (2010).

[9] Y. Zhou, M. M. Alam, H. X. Yang, H. Guo and D. H. Wood, "Fluid forces on a very low Reynolds number airfoil and their prediction," Int J Heat Fluid Fl **32** (1), 329-339 (2011).

[10] P. Kunz and I. Kroo, "Analysis, design, and testing of airfoils for use at ultra-low Reynolds numbers," in *Fixed, flapping and rotary wing vehicles at very low Reynolds numbers*, edited by T. J. Mueller (AIAA, Reston, Virginia, 2001).

[11] P. J. Mckeough and J. M. R. Graham, "Effect of mean loading on the fluctuating loads induced on aerofoils by a turbulent stream," Aeronaut Quart **31** (Feb), 56-69 (1980).

[12] J. A. Hoffmann, "Effects of freestream turbulence on the performance characteristics of an airfoil," AIAA J **29** (9), 1353-1354 (1991).

[13] P. F. Mish and W. J. Devenpor, "Mean loading effects on the surface pressure fluctuations on an airfoil in turbulence," AIAA Paper No. 2001-2211 (2001).

[14] L. Gilling, N. S rensen and L. Davidson, "Detached eddy simulations of an airfoil in turbulent inflow," AIAA Paper No. 2009-270 (2009).

[15] R. F. Huang and H. W. Lee, "Effects of freestream turbulence on wing-surface flow and aerodynamic performance," J Aircraft **36** (6), 965-972 (1999).

[16] P. Devinant, T. Laverne and J. Hureau, "Experimental study of wind-turbine airfoil aerodynamics in high turbulence," J Wind Eng Ind Aerod **90** (6), 689-707 (2002).

[17] J. Colman, J. M. Di Leo, J. S. Delnero, M. Martinez, U. Boldes and F. Bacchi, "Lift and drag coefficients behaviour at low Reynolds number in an airfoil with gurney flap submitted to a turbulent flow. Part 1," Lat Am Appl Res **38** (3), 195-200 (2008).

[18] H. F. Wang, Y. Zhou, C. K. Chan and K. S. Lam, "Effect of initial conditions on interaction between a boundary layer and a wall-mounted finite-length-cylinder wake," Phys Fluids **18** (6), 065106 (2006).

[19] J. Hoffmann, "Effects of onset free-stream turbulence on the performance characteristics of an airfoil," AIAA Paper No. 1990-3025 (1990).

[20] C. Sicot, S. Aubrun, S. Loyer and P. Devinant, "Unsteady characteristics of the static stall of an airfoil subjected to freestream turbulence level up to 16%," Exp Fluids **41** (4), 641-648 (2006).

[21] E. C. Maskell, "A theory of the blockage effects on bluff bodies and stalled wings in a closed wind tunnel," Aeronautical Research Council Reports and Memoranda No.3400 (1963).

[22] J. B. Barlow, W. H. Rae and A. Pope, *Low-speed wind tunnel testing*, 3rd ed. (Wiley, 1999).

[23] W. J. McCroskey, "A critical assessment of wind tunnel results for the NACA 0012 airfoil," NASA TM No.100019 (1987).

[24] A. Host-Madsen and D. McCluskey, "On the accuracy and reliability of piv measurements," DTIC Report No. ADA285647, 26.4.1-26.4.11 (1994).

[25] S. Sunada, K. Kawachi, K. Yasuda and T. Yasuda, "Comparison of wing characteristics at an ultralow Reynolds number," J Aircraft **39** (2), 331-338 (2002).

[26] D. J. Cleaver, Z. Wang, I. Gursul and M. R. Visbal, "Lift enhancement by means of small-amplitude airfoil oscillations at low Reynolds numbers," AIAA J **49** (9), 2018-2033 (2011).

[27] C. C. Critzos, H. H. Heyson and J. Boswinkle, Robert W., "Aerodynamic characteristics of NACA 0012 airfoil section at angles of attack from 0 to 180 degrees," NACA TN No. 3361 (1955).

[28] M. M. Munk, "Elements of the wing section theory and of the wing theory," NACA Report No. 191 (1924).

[29] J. Panda and K. B. M. Q. Zaman, "Experimental investigation of the flow field of an oscillating airfoil and estimation of lift from wake surveys," J Fluid Mech **265**, 65-95 (1994).

[30] E. V. Laitone, "Wind tunnel tests of wings at Reynolds numbers below 70 000," Exp Fluids **23** (5), 405-409 (1997).

[31] T. Lutz, W. Würz and S. Wagner, "Numerical optimization and wind-tunnel testing of low Reynolds number airfoils," in *Fixed, flapping and rotary wing vehicles at very low Reynolds numbers*, edited by T. J. Mueller (AIAA, Reston, Virginia, 2001).

[32] E. N. Jacobs and A. Sherman, "Airfoil section characteristics as affected by variations of the Reynolds number," NACA Report No. 586 (1937).

[33] D. E. Gault, "A correlation of low-speed, airfoil-section stalling characteristics with Reynolds number and airfoil geometry," NACA TN No. 3963 (1957).

[34] E. C. Polhamus, "A survey of Reynolds number and wing geometry effects on lift characteristics in the low speed stall region," NASA CR No. 4745 (1996).

[35] J. M. Chen and C.-c. Choa, "Freestream disturbance effects on an airfoil pitching at constant rate," J Aircraft **36** (3), 507-514 (1999).

[36] T. Grager, A. Rothmayer and H. Hu, "Stall suppression of a low-Reynolds-number airfoil with a dynamic burst control plate," AIAA Paper No. 2011-1180 (2011).

[37] T. Lee and P. Gerontakos, "Investigation of flow over an oscillating airfoil," J Fluid Mech **512**, 313-341 (2004).

[38] C. Wong and K. Kontis, "Flow control by spanwise blowing on a NACA 0012," J Aircraft **44** (1), 338-341 (2007).

[39] R. Sant, L. Ayuso and J. Meseguer, "Aerodynamic study of airfoils geometric imperfections at low Reynolds number," AIAA Paper No. 2011-1256 (2011).

[40] G. B. McCullough and D. E. Gault, "Examples of three representative types of airfoil section stall at low speeds," NACA TN No. 2502 (1951).

[41] D. R. Chapman, D. M. Kuehn and H. K. Larson, "Preliminary report on a study of separated flows in supersonic and subsonic streams," NACA RM No. A55L14 (1956).

[42] M. S. H. Boutilier and S. Yarusevych, "Parametric study of separation and transition characteristics over an airfoil at low Reynolds numbers," Exp Fluids **52** (6), 1491-1506 (2012).

[43] P. F. Mish and W. J. Devenport, "An experimental investigation of unsteady surface pressure on an airfoil in turbulence—part 1: Effects of mean loading," J Sound Vib **296**

(3), 417-446 (2006).

[44] P. F. Mish and W. J. Devenport, "An experimental investigation of unsteady surface pressure on an airfoil in turbulence—part 2: Sources and prediction of mean loading effects," J Sound Vib **296** (3), 447-460 (2006).

[45] S. Yarusevych, J. G. Kawall and P. E. Sullivan, "Separated-shear-layer development on an airfoil at low Reynolds numbers," AIAA J **46** (12), 3060-3069 (2008).

[46] S. Sunada, A. Sakaguchi and K. Kawachi, "Airfoil section characteristics at a low Reynolds number," Journal of Fluids Engineering **119** (1), 129-135 (1997).

[47] H. L. Dryden and A. M. Kuethe, "Effect of turbulence in wind tunnel measurements," NACA Report No. 342 (1931).

[48] E. N. Jacobs and W. C. Clay, "Characteristics of the NACA 23012 airfoil from tests in the full-scale and variable-density tunnels," NACA Report No. 530 (1936).

[49] R. C. Platt, "Turbulence factors of NACA wind tunnels as determined by sphere tests," NACA Report No. 558 (1936).

[50] B. H. Carmichael, "Low Reynolds number airfoil survey, volume 1," NASA CR No. 165803 (1981).

[51] R. F. Huang and C. L. Lin, "Vortex shedding and shear-layer instability of wing at low-Reynolds numbers," AIAA J **33** (8), 1398-1403 (1995).

[52] D. Olson, A. Katz, A. Naguib, M. Koochesfahani, D. Rizzetta and M. Visbal, "On the challenges in experimental characterization of flow separation over airfoils at low Reynolds number," Exp Fluids **54** (2), 1-11 (2013).

[53] C. D. Aubertine, Ph.D. thesis, Stanford University, 2005.

[54] H. Hu and M. Tamai, "Bioinspired corrugated airfoil at low Reynolds numbers," J Aircraft **45** (6), 2068-2077 (2008).

[55] K. Hord and Y. Lian, " Numerical investigation of the aerodynamic and structural characteristics of a corrugated airfoil," J Aircraft **49** (3), 749-757 (2012).

[56] M. Gaster, "The structure and behaviour of laminar separation bubbles," A.R.C. R.&M. No. 5395. (1967)

[57] M. Drela and M. B. Giles, “Viscous-inviscid analysis of transonic and low Reynolds number airfoils,” AIAA J **25 (**10), 1347–1355 (1987).